

THE UNIVERSITY OF CHICAGO

FUTURE COSMIC MICROWAVE BACKGROUND DELENSING WITH GALAXY  
SURVEYS

A DISSERTATION SUBMITTED TO  
THE FACULTY OF THE DIVISION OF THE PHYSICAL SCIENCES  
IN CANDIDACY FOR THE DEGREE OF  
DOCTOR OF PHILOSOPHY

DEPARTMENT OF ASTRONOMY AND ASTROPHYSICS

BY  
ALESSANDRO MANZOTTI

CHICAGO, ILLINOIS

AUGUST 2017

Copyright © 2017 by Alessandro Manzotti  
All Rights Reserved

# TABLE OF CONTENTS

LIST OF FIGURES . . . . .	iv
LIST OF TABLES . . . . .	vi
ABSTRACT . . . . .	vii
1 INTRODUCTION . . . . .	1
2 LENSING POTENTIAL TRACERS . . . . .	4
2.0.1 CMB lensing potential . . . . .	4
2.0.2 Galaxies . . . . .	5
2.0.3 Cosmic infrared Background (CIB) . . . . .	7
3 GRAVITATIONAL LENSING B-MODE AND DELENSING . . . . .	8
3.0.1 Single tracer of the lensing potential . . . . .	9
3.0.2 Multiple tracers of the lensing potential . . . . .	11
3.0.3 Improving efficiency with tomographic binning . . . . .	13
4 PARAMETER CONSTRAINTS IMPROVEMENT AFTER DELENSING . . . . .	18
4.0.1 Fisher Information Matrix . . . . .	18
4.0.2 Delensing with current CMB and LSS . . . . .	20
4.0.3 CMB-S3 Era . . . . .	25
4.0.4 CMB-S4 Era . . . . .	28
5 CONCLUSIONS . . . . .	33
6 ACKNOWLEDGMENTS . . . . .	36
REFERENCES . . . . .	37

## LIST OF FIGURES

3.1	Here we illustrate the effect of delensing on the B-mode power spectrum. The orange solid line corresponds to the fiducial lensing B-mode component of the signal while the dashed blue line corresponds to the inflationary one for the higher amplitude allowed by current experiments. These are compared with the residual power left after delensing using some of the LSS tracers described in section 2. The rapid improvement in the level of instrumental noise (dashed curves for SPTPol and CMB S4) will require a high delensing efficiency to exploit these experiments fully. . . . .	12
3.2	Kernel Comparison: Comparison of the different kernels as a function of redshift for some of the tracers used in this analysis. The bigger the overlap with the CMB lensing kernel the better the reconstruction of the lensing potential is thus leading to a higher delensing efficiency. . . . .	14
3.3	Comparison of kernels of the 10 LSST tomographic bins together with the full LSST survey and the CMB lensing kernel. Compared to a full survey approach, tomographic binning allows to optimally weight different bins according to their cross-correlation with the CMB lensing. This leads to a better delensing efficiency. . . . .	16
3.4	Tomographic bins improve the cross-correlation of galaxy surveys with CMB lensing. Here we show the cross-correlation coefficient (Eq. (3.10)) as a function of angular scale for full surveys (solid lines) and tomographically binned surveys (dot-dashed line). For details about the binning, see section 3.0.3 and in particular Eq. (3.16). . . . .	17
4.1	Correlation factor $\rho$ with the CMB lensing potential as a function of the angular scale $\ell$ for completed and ongoing Stage-2 tracers. Here we show both current galaxy survey and internally reconstructed CMB lensing potential. The dashed curve highlights which scales contribute to the $\ell < 100$ B-mode power and are thus most useful to delens. It corresponds to (with arbitrary scale) $C^{\kappa\kappa} \times \frac{\partial C^{BB}}{\partial C^{\kappa\kappa}}$ . . . . .	22
4.2	Correlation factor $\rho$ with the CMB lensing potential as a function of the angular scale $\ell$ for completed and ongoing Stage-2 tracers. This figure is the same as Fig. 4.1 but using SPTPol instead of Planck as the high-res CMB experiment performing the internal reconstruction. . . . .	23
4.3	Correlation factor $\rho$ with the CMB lensing potential as a function of the angular scale $\ell$ . This figure is the same as Fig. 4.2 but with a stage-3 CMB experiment performing the internal reconstruction and with DESI added to the stage-2 galaxy surveys (LSS-S2). . . . .	27
4.4	Correlation factor $\rho$ with the CMB lensing potential as a function of the angular scale $\ell$ . This figure is the same as Fig. 4.2 but with a stage-4 CMB experiment performing the internal reconstruction and with LSST and SKA added to the stage-2 and stage-3 galaxy surveys (LSS-S3). . . . .	29

4.5	Correlation factor $\rho$ with the CMB lensing potential as a function of the angular scale $\ell$ . This figure is the same as Fig. 4.2 but with a stage-4 CMB experiment performing the internal reconstruction and with LSST and SKA added to the stage-2 and stage-3 galaxy surveys (LSS-S3). . . . .	30
5.1	Summary of the amount of lensing B-modes power removed by different tracers for different generations of experiments. The bars on the left represent the individual contribution of different galaxy tracers. On the right, the gray bar represents the contribution from LSS only and the yellow one the total removed power once LSS and CMB internal reconstruction are combined. The values are taken from Tab. 4.1, Tab. 4.2, Tab. 4.3 and Tab. 4.4. . . . .	35

## LIST OF TABLES

4.1	$\alpha(r)$ : Improvements on $\sigma(r)$ due to delensing for completed and ongoing Stage-2 surveys and Planck lensing reconstruction. LSS-S2 corresponds to the combination of all the available LSS tracers. The values in parenthesis in the first column correspond to the fraction of lensing B-mode power removed using each LSS tracer. The values in the other columns correspond to ratio of the error before and after delensing for 3 cases: no instrumental noise in the B-mode measurement and realistic noise for two different values of $r$ . . . . .	25
4.2	$\alpha(r)$ : Stage-2 improvements on $\sigma(r)$ due to delensing. We use the same LSS tracers as Tab. 4.1 but with the internal lensing reconstruction performed by SPTPol. . . . .	25
4.3	$\alpha$ : Improvements on $\sigma(r)$ due to delensing for S3 experiments. Here we define LSS-S3 as the combination of S2 LSS tracers (LSS-S2) and DESI. We also use a CMB S3 experiment for the lensing internal reconstruction. See section 4.0.3 for details. . . . .	27
4.4	$\alpha$ : Improvements on $\sigma(r)$ due to delensing for S4 experiments. Here we define LSS-S4 as the combination of S3 LSS tracers (LSS-S3) and LSST. We also consider SKA-like radio-continuum surveys. We also use a CMB S4 experiment for the lensing internal reconstruction. See section 4.0.4 for details. . . . .	32

# ABSTRACT

The cosmic microwave background (CMB) polarization is a promising experimental dataset to test the inflationary paradigm and to probe the physics of the early universe. A particular component, the so-called B-modes, is indeed a direct signature of a prediction of inflation: the presence of gravitational waves in the early universe. However, reducing the instrumental noise in future experiments will not be enough to detect this signal. Secondary effects in the low redshift universe will also produce non-primordial B-modes adding confusion to the inflationary signal. In particular, the gravitational interactions of CMB photons with large scale structures will distort the primordial E-modes adding a lensing B-mode component to the primordial signal. Removing the lensing part (“delensing”) from the measurement of CMB B-modes will then be necessary to constrain the amplitude of the primordial gravitational waves. Here we discuss the role of current and future large scale structure surveys in a multi-tracers approach to delensing that will improve the reconstruction of the lensing potential that lenses the CMB photons and, as a consequence, the delensing efficiency. We quantify this by the improvement due to delensing on the constraints on the inflationary tensor perturbations amplitude and shape ( $r$  and  $n_t$ ). We find that, in general, galaxy surveys should be split into tomographic bins as this can improve the correlation with CMB lensing by 30%. Among currently available surveys, a DES-like galaxy survey can remove about 14% of the lensing signal. Ongoing CMB experiments (CMB-S2) will particularly benefit from large scale structure tracers that, once properly combined, will have a better performance than a CMB internal reconstruction. With the decrease of instrumental noise, the CMB internal reconstruction will increase its efficiency and the fraction of removed lensing B-modes with CMB alone will rapidly improve from the current level of Planck (8%) and SPTPol (35%) to 3G (56%) and CMB S4 (85%) level. Nevertheless optical galaxy surveys will still play an important role even for CMB S4. In particular an LSST-like survey can achieve a delensing performance comparable to a 3G CMB experiment but with completely

different systematics. This will be important to prove the robustness against systematics of an eventual detection of primordial B-modes.

# CHAPTER 1

## INTRODUCTION

In the standard cosmological paradigm the early universe underwent a period of near-exponential expansion called “cosmic inflation”. All the cosmological observations agree with this picture, making it a compelling and elegant description of the Universe initial conditions. Despite the experimental effort, other possible explanations are still valid, and a conclusive evidence of inflation is still to be found. Inflation generically predicts a stochastic background of gravitational waves [see e.g. 15, for a review]. This prediction sets inflation apart from other theories and a detection of primordial gravitational waves could be the compelling evidence cosmologists are looking for. These primordial gravitational waves in the early universe would imprint a unique signature on the polarized anisotropies of the CMB. For this reason, CMB polarization is a promising dataset to understand the physics of the early universe and ultimately test inflation. In particular, we can decompose the CMB polarization fields in Fourier space into even-parity (divergence) and odd-parity (curl) components, referred to as “E” and “B” modes. In the standard scenario, the B-mode polarization is a clean probe of primordial gravitational waves, because these are the only source of B-modes at the epoch of recombination.

Because the CMB B-modes provide the cleanest known observational window into the primordial gravitational wave background, improving their measurement is a major objective of current and future CMB experiments. Even if inflationary B-modes have not been detected yet, the target value  $r \gtrsim 10^{-3}$ , should be reachable shortly given the level of noise expected in future CMB experiments [15, 1]. However, just reducing the level of noise will not be enough to attain this goal. Indeed, the observed B modes are not solely sourced by early universe physics; they are also produced by secondary effects taking place in the late-time low-redshift universe. In this work, we will focus on the effect of gravitational interactions with large scale structures (LSS). Lensing shears the CMB polarization pattern, producing “lensing B

modes” from CMB E modes [49]. This expected component has now been measured both in cross-correlation with LSS [12, 5, 35, 45, 31] and from CMB data alone [34, 4, 17].

This component acts as a source of confusion for searches of the primordial gravitational wave background. Indeed, the contamination from lensing B modes is already at the level of the instrumental noise of current experiments [16]. Thus, together with the experimental effort to reduce the amount of noise, the effect of the lensing component must be understood.

The optimal way to reduce the lensing contributions to the B-modes is to reconstruct a template of the actual lensing B modes on the observed part of the sky and then use it to clean the data in a process called “delensing”. We can delens the observed B-modes by combining CMB polarization data (what is *lensed*) with tracers of the large scale structure (what is *lensing*) to reconstruct a template of the expected lensing B-modes. Delensing has been studied for many years [20, 18, 38, 42, 40, 43]. Furthermore, it has recently been performed on CMB temperature data using the cosmic infrared background (CIB) as LSS tracer [21] and on CMB temperature and polarization data using CMB data to internally reconstruct the LSS lensing potential [7]. Finally, the highest B-mode delensing efficiency has been achieved with SPT and Herschel data in which 28% of the lensing power was removed [26].

For future experiments, we need to increase the delensing efficiency by almost a factor of 3 to fully exploit the expected instrumental capabilities [1]. In this paper, we propose and study a possible way: using future galaxy surveys as tracers of the lensing potential in addition to other probes such as the SKA radio continuum survey, cosmic infrared background and internal CMB reconstruction. Furthermore, we point out how using redshift information through tomographic binning can improve the delensing efficiency of galaxy survey. These will translate into a better reconstruction of the B-modes in the measured patch, and, as a consequence will improve the constraints on inflation through delensing. We model several actual and future surveys, and after computing the residual B-modes, we forecast the

resulting statistical uncertainties on the amplitude and the shape of the inflationary tensor perturbations for current CMB experiments as well as the next generation (S3) and the planned fourth generation (S4).

We organize this article as follows: we describe the LSS tracers used in this analysis in section 2. In section 3 we define the lensing B-mode component and the residual power after delensing with tracers of the lensing potential. The main result of this work is presented in section 4 : the improvement of inflationary parameters constraints due to delensing with CMB and LSS. We conclude in section 5.

## CHAPTER 2

### LENSING POTENTIAL TRACERS

In this section, we introduce the different large scale structure tracers considered in this work to reconstruct the lensing potential. Gravitational lensing distorts primordial E-modes generating a non-primordial B-mode component. Also, we define the power spectra that we will use later in section 3.

Large scale structure surveys usually probe the 3D matter overdensities as a 2D field projected along the line of sight:

$$\delta^i(\hat{\mathbf{n}}) = \int_0^\infty dz W^i(z) \delta(\chi(z)\hat{\mathbf{n}}, z). \quad (2.1)$$

where  $\delta(\chi(z)\hat{\mathbf{n}}, z)$  corresponds to the dark matter overdensity field at a comoving distance  $\chi(z)$  and at a redshift  $z$  in the angular direction  $\hat{\mathbf{n}}$ . Using the Limber approximation [24] we can compute the power spectra of two large-scale structure fields  $i, j$  as:

$$C_\ell^{ij} = \int_0^\infty \frac{dz}{c} \frac{H(z)}{\chi(z)^2} W^i(z) W^j(z) P(k, z). \quad (2.2)$$

In this equation,  $H(z)$  is the Hubble factor at redshift  $z$ ,  $c$  is the speed of light, and  $P(k, z)$  is the matter power spectrum evaluated at wavenumber  $k = \ell/\chi(z)$  and redshift  $z$ . We will now describe the kernels  $W^i(z)$  for each of the tracers used in this work.

#### *2.0.1 CMB lensing potential*

We start from the CMB lensing potential. The lensing kernel  $W^\kappa$  is:

$$W^\kappa(z) = \frac{3\Omega_m}{2c} \frac{H_0^2}{H(z)} (1+z) \chi(z) \frac{\chi_* - \chi(z)}{\chi_*}, \quad (2.3)$$

where  $\chi_*$  is the comoving distance to the last-scattering surface at  $z_* \simeq 1090$ ,  $\Omega_m$  and  $H_0$  are the present day values of the Hubble and matter density parameters, respectively. As can be seen in Fig. 3.2, the lensing kernel  $W^\kappa(z)$  is a broad function of redshift peaking around  $z = 1.8$  but extending to high redshift.

The CMB lensing potential is *the* field that we need in order to reverse the effect of large scale structure and delens the CMB. However, the lensing potential can also be reconstructed using the CMB itself. In that case, we can treat it as a noisy tracer of the true field. Both the CMB lensing field and its noisy reconstructed counterpart have the same kernel  $W^\kappa(z)$ . However, when computing the power spectrum of the latter, we need to add a noise component. Given the instrumental noise level and the beam, we can calculate the reconstruction noise  $N_\ell^{\kappa\kappa}$ , and so

$$C_l^{\kappa_{\text{rec}}\kappa_{\text{rec}}} = C_l^{\kappa\kappa} + N_\ell^{\kappa\kappa} \quad (2.4)$$

In this work, the level of noise is computed assuming an iterative approach to the CMB lensing reconstruction as described in [43, 13].

### 2.0.2 Galaxies

The galaxy clustering kernel is:

$$W^g(z) = \frac{b(z) \frac{dN}{dz}}{\left( \int dz' \frac{dN}{dz'} \right)}. \quad (2.5)$$

Here  $\frac{dN}{dz}$  is the number of galaxies observed by the survey as a function of redshift while  $b(z)$  is the galaxy bias that connects the amplitude of galaxy overdensities to the underlying dark matter density. We use a linear bias independent of the angular scale, which is a reasonable assumption for the relatively large scales relevant for delensing ( $\ell < 1000$ ). When computing

the auto-spectrum of the galaxy density, a shot noise term needs to be taken into account. To do so, we add a constant term to the power spectrum equal to the inverse of the number of galaxies per steradians. Different galaxy surveys in this work are then fully characterized by their  $b(z)$ ,  $\frac{dN}{dz}$  and the observed galaxy density. We test the delensing efficiency taking into account both current surveys like WISE or DES as well as future galaxy surveys like DESI and LSST as well as 21 cm measurement like SKA.

The WISE survey observed the entire sky in the infrared [46]. We defined the redshift distribution of the WISE infrared galaxy samples following [47] (see Fig. 4 therein). To compute the noise term, we assume that the available sky after masking is around  $f_{sky} = 0.44$  with 50 million galaxies [9] and that the galaxy density is approximately uniform. Furthermore we adopt a linear bias  $b_{\text{WISE}} = 1.41$  obtained by [9] cross correlating WISE with Planck lensing potential.

DES is modeled after the DES Science Verification public data release. For DESI we used the  $\frac{dN}{dz}$  in Tab. 2.3 of the DESI Technical Design Report. From that we can derive the galaxy density of 0.63 galaxies per squared arcmin.

For LSST we follow [36]:  $\frac{dN}{dz} \propto z^\alpha \exp^{-(z/z_0)^\beta}$  with  $\alpha = 1.27$ ,  $\beta = 1.02$ , and  $z_0 = 0.5$ . Furthermore we assume a density of 26 galaxies per arcmin squared.

Finally, we consider the Square Kilometre Array (SKA). The SKA is a planned radio array that will survey large scale structure primarily by detecting the redshifted neutral hydrogen (HI) 21cm emission line from a large number of galaxies out to high redshift. We will assume an intensity mapping survey mode where SKA will measure the large-scale fluctuations of the *integrated* 21cm intensity from many unresolved galaxies. We model both the redshift distribution and bias of radio sources following [29]. In Fig. 3.2, we compare the CMB lensing kernel  $W^\kappa(z)$  to the kernels  $W^g(z)$  of all the tracers introduced here.

### 2.0.3 Cosmic infrared Background (CIB)

The CIB consists of diffuse extragalactic radiation generated by the unresolved emission from star-forming galaxies (see [8] and references therein). In these galaxies, the UV light from young stars heats the dust regions around them that then reradiates thermally in the infrared with a graybody spectrum of  $T \simeq 30\text{K}$ .

Following [2], we model the CIB power directly as  $C_\ell^{\text{CIB-CIB}} = 3500(l/3000)^{-1.25} \text{Jy}^2/\text{sr}$ . This model provides an accurate fit to several experimental results. For the cross-spectra with the CMB lensing or other galaxy tracers,  $C_\ell^{\text{CIB-}j}$ , we use the single-SED model of [11]. It corresponds to the kernel:

$$W^{\text{CIB}}(z) = b_c \frac{\chi^2(z)}{H(z)(1+z)^2} e^{-\frac{(z-z_c)^2}{2\sigma_z^2}} f_{\nu(1+z)}, \quad (2.6)$$

for

$$f_\nu = \begin{cases} \left(e^{\frac{h\nu}{kT}} - 1\right)^{-1} \nu^{\beta+3} & (\nu \leq \nu') \\ \left(e^{\frac{h\nu'}{kT}} - 1\right)^{-1} \nu'^{\beta+3} \left(\frac{\nu}{\nu'}\right)^{-\alpha} & (\nu > \nu') \end{cases} \quad (2.7)$$

We place the peak of the CIB emissivity at redshift  $z_c = 2$  with a broad redshift kernel of width  $\sigma_z = 2$  and we set  $T = 34\text{K}$  and  $\nu' \approx 4955 \text{ GHz}$ . Fig. 3.2 shows how the CIB kernel peaks at higher redshift compared to other galaxy survey kernels, with a better overlap with the CMB lensing one.

There are several available CIB observations that have already been used to delens the CMB. Given its full-sky coverage, a promising one is the CIB map derived in [33] using multi-frequency Planck data and the Generalized Needlet Internal Linear Combination (GNILC) component separation algorithm.

## CHAPTER 3

### GRAVITATIONAL LENSING B-MODE AND DELENSING

The large scale structures described in section 2 have an important impact on the search of primordial CMB B-modes: they lens the primordial E-modes generating non inflationary B-modes that, then constitute an important source of noise.

Indeed the Q and U mode decompositions of the CMB photons polarization are remapped by lensing as:

$$Q(\hat{\mathbf{n}}) = Q_{\text{unlensed}}(\hat{\mathbf{n}} + \nabla\phi); \quad U(\hat{\mathbf{n}}) = U_{\text{unlensed}}(\hat{\mathbf{n}} + \nabla\phi) \quad (3.1)$$

where the deflection angle is the gradient of the lensing potential integrated along the line of sight  $\nabla\phi$ . The CMB polarization is usually decomposed into odd-parity Fourier modes E and B. As shown in [39], because of the symmetry of the problem, tensor perturbations are the principal source of the B-modes configuration. For this reason, B-modes are a promising signature of early universe tensor perturbations.

However, this promising sign of primordial gravitational waves is partially obscured by gravitational interactions with large scale structures that generate CMB B-modes by distorting primordial E-modes. At first order, given the convergence field  $\kappa = -\frac{1}{2}\nabla^2\phi$  introduced in section 2.0.1 the B-modes resulting from the lensing of the primordial E-modes are:

$$B^{\text{lens}}(\mathbf{l}) = \int \frac{d^2\mathbf{l}'}{(2\pi)^2} W(\mathbf{l}, \mathbf{l}') E(\mathbf{l}') \kappa(\mathbf{l} - \mathbf{l}') \quad (3.2)$$

where different modes contributes with a different weight:

$$W(\mathbf{l}, \mathbf{l}') = \frac{2\mathbf{l}' \cdot (\mathbf{l} - \mathbf{l}')}{|\mathbf{l} - \mathbf{l}'|^2} \sin(2\varphi_{\mathbf{l}, \mathbf{l}'}). \quad (3.3)$$

Here  $\varphi_{\mathbf{l}, \mathbf{l}'}$  is the angle between the two different modes  $\mathbf{l}$  and  $\mathbf{l}'$ . From this we get the power

spectrum of the lensing component of the B-modes:

$$C_\ell^{BB,\text{lens}} = \int \frac{d^2\mathbf{l}'}{(2\pi)^2} W^2(\mathbf{l}, \mathbf{l}') C_{\mathbf{l}'}^{EE} C_{|\mathbf{l}-\mathbf{l}'|}^{\kappa\kappa}. \quad (3.4)$$

The B-mode power spectrum measured on the sky is composed of a possible primordial component  $C_\ell^{BB,r}$  together with the lensing  $C_\ell^{BB,\text{lens}}$  contribution and the instrumental noise  $N_\ell^{BB}$  (defined in Eq. (4.3)):

$$C_\ell^{BB,\text{measured}} = C_\ell^{BB,r} + C_\ell^{BB,\text{lens}} + N_\ell^{BB}. \quad (3.5)$$

The lensing component is a significant source of B-modes that, at large scales, corresponds to a white noise source of roughly  $5\mu K\text{-arcmin}$  independent of the angular scale. This means that it is not only larger than the allowed inflationary component at scales smaller than several degrees, but it is also comparable to current levels of instrumental noise. For this reason, it is critical to characterize and eventually remove it from the data. To do so, we build a template Eq. (3.2) of the lensing B-modes in the observed patch given a measurement of the E-mode field and the lensing potential  $\phi$ . While E is measured directly, we can estimate  $\phi$  using "tracers" of the matter distribution that sources the potential.

### 3.0.1 *Single tracer of the lensing potential*

We will now show how the delensing efficiency is related to the fidelity of the lensing tracers and the instrumental noise in the CMB E-modes. If we have a large scale structure field  $\mathbf{I}(\hat{\mathbf{n}})$  that traces the lensing potential we can build a template of the lensing B-modes on the sky by a weighted convolution:

$$\hat{B}^{\text{lens}}(\mathbf{l}) = \int \frac{d^2\mathbf{l}'}{(2\pi)^2} W(\mathbf{l}, \mathbf{l}') f(\mathbf{l}, \mathbf{l}') E^N(\mathbf{l}') I(\mathbf{l} - \mathbf{l}'), \quad (3.6)$$

where  $f(\mathbf{l}, \mathbf{l}')$  can be determined by minimizing the difference with the true  $B^{\text{lens}}(\mathbf{l})$  defined in Eq. (3.2). We include the instrumental noise in the CMB E-modes ( $E^N$ ) that will also limit the ability to fully reconstruct the lensing B-modes.

The residual lensing B-modes due to an imperfect knowledge of the true E-mode and  $\phi$  will be

$$B^{\text{res}}(\mathbf{l}) = B^{\text{lens}}(\mathbf{l}) - \hat{B}^{\text{lens}}(\mathbf{l}) = \int \frac{d^2\mathbf{l}'}{(2\pi)^2} W(\mathbf{l}, \mathbf{l}') \times \left( E(\mathbf{l}') \kappa(\mathbf{l} - \mathbf{l}') - f(\mathbf{l}, \mathbf{l}') E^N(\mathbf{l}') I(\mathbf{l} - \mathbf{l}') \right). \quad (3.7)$$

The optimal weights  $f(\mathbf{l}, \mathbf{l}')$ , chosen such that the residual lensing B mode power is minimized, are:

$$f(\mathbf{l}, \mathbf{l}') = \left( \frac{C_{\mathbf{l}'}^{EE}}{C_{\mathbf{l}'}^{EE} + N_{\mathbf{l}'}^{EE}} \right) \frac{C_{|\mathbf{l}-\mathbf{l}'|}^{\kappa I}}{C_{|\mathbf{l}-\mathbf{l}'|}^{II}}. \quad (3.8)$$

Here  $C^{\kappa I}$  and  $C^{II}$  are the cross-correlation spectrum of the tracer  $I$  with the lensing convergence  $\kappa$  and its autospectrum; they are described for each LSS field in section 2. The power spectrum of the E-modes noise  $N^{EE}$  is the same as the B-modes one in Eq. (4.3).

With this choice of  $f(\mathbf{l}, \mathbf{l}')$  we find that the residual power is:

$$C_l^{BB, \text{res}} = \int \frac{d^2\mathbf{l}'}{(2\pi)^2} W^2(\mathbf{l}, \mathbf{l}') C_{\mathbf{l}'}^{EE} C_{|\mathbf{l}-\mathbf{l}'|}^{\kappa\kappa} \times \left[ 1 - \left( \frac{C_{\mathbf{l}'}^{EE}}{C_{\mathbf{l}'}^{EE} + N_{\mathbf{l}'}^{EE}} \right) \rho_{|\mathbf{l}-\mathbf{l}'|}^2 \right] \quad (3.9)$$

with

$$\rho_{\ell}^2 = \frac{(C_l^{\kappa I})^2}{C_l^{\kappa\kappa} C_l^{II}}. \quad (3.10)$$

Eq. (3.9) highlights the different factors that control the delensing efficiency. The first part of the second term in the parenthesis consists of an inverse variance filter applied to the measured E-mode. The smaller the noise in the E-modes ( $N^{EE}$ ) is the closer this term is to

one: a less noisy measurement improves the template of the lensing B-modes. The second captures the difference between the reconstructed  $\phi$  and the CMB lensing potential, and it directly relates the residual power after delensing with the cross-correlation coefficients with CMB lensing of the tracers used. The larger the  $\rho_\ell^2$  is for an LSS field, the more it is correlated with the lensing potential acting on the CMB photons. A higher correlation allows for a better reconstruction of  $\phi$  and, as a consequence, of  $B^{\text{lens}}$  leading to a smaller residual power  $C_l^{BB,\text{res}}$ . We conclude this section showing in Fig. 3.1 the expected residual lensing B-modes power spectrum for some of the tracers used in this work together with the primordial B-modes component and the instrumental noise for current and future experiments.

### 3.0.2 Multiple tracers of the lensing potential

In this section we extend the formalism to the case where multiple tracers are used to reconstruct the lensing potential.

We start by assuming that we have  $n$  different tracers of the gravitational potentials  $I_i$  with  $i \in \{1, \dots, n\}$ . We can optimally combine them to estimate  $\phi$  or, in other words, to maximize the correlation factor  $\rho$  with:

$$\begin{aligned} I &= \sum_i c^i I^i \\ c_i &= (C_{II}^{-1})_{ij} C^{\kappa I^j} \end{aligned} \tag{3.11}$$

where  $C_{II}$  is the covariance matrix of the LSS tracers. The residual B-mode power can be derived from Eq. (3.9) using an “effective” correlation  $\rho^2$  of these combined tracers with gravitational lensing:

$$\rho_\ell^2 = \sum_{i,j} \frac{C_\ell^{\kappa^i} (C_\ell^{-1})_{ij} C_\ell^{\kappa^j}}{C_\ell^{\kappa\kappa}}. \tag{3.12}$$

Note that the gain in adding a new tracer is not only proportional to its correlation with

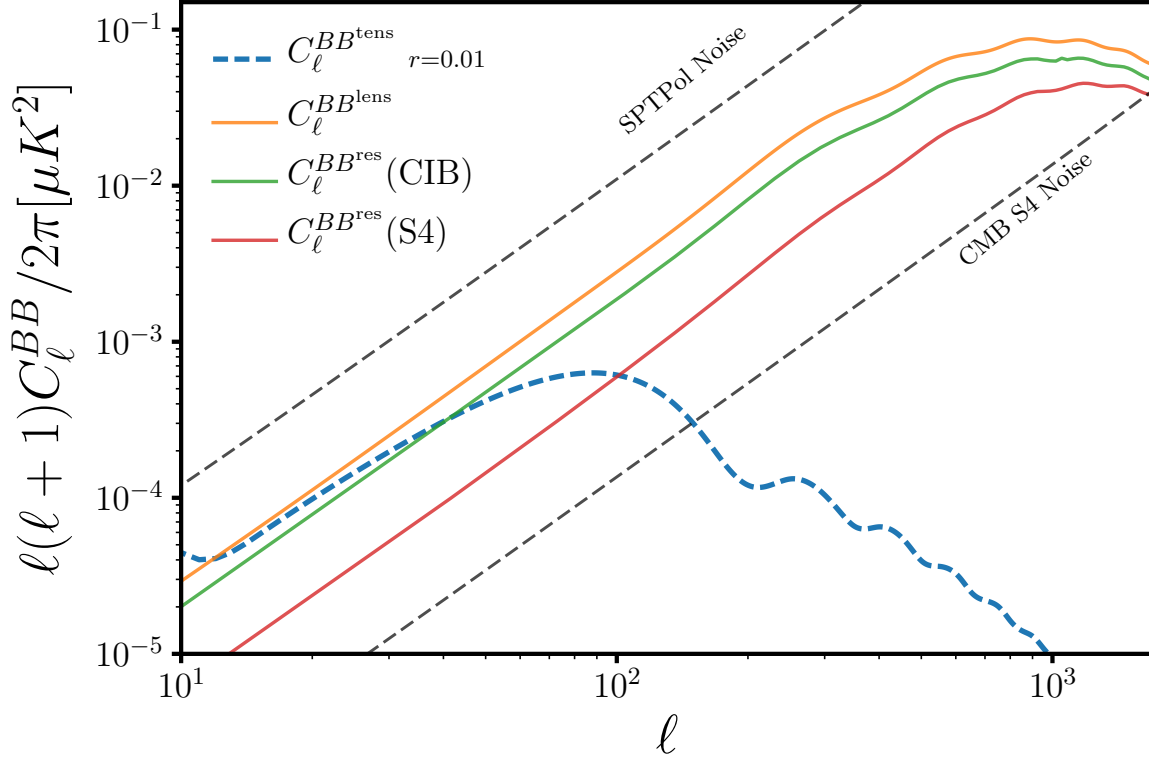


Figure 3.1: Here we illustrate the effect of delensing on the B-mode power spectrum. The orange solid line corresponds to the fiducial lensing B-mode component of the signal while the dashed blue line corresponds to the inflationary one for the higher amplitude allowed by current experiments. These are compared with the residual power left after delensing using some of the LSS tracers described in section 2. The rapid improvement in the level of instrumental noise (dashed curves for SPTPol and CMB S4) will require a high delensing efficiency to exploit these experiments fully.

the CMB lensing, but it also depends on how much it is correlated with the already used set of tracers. Fig. 3.2 show the different kernels as a function of redshift computed using the models and parameters described in section 2. The cross-correlation of a tracer with the CMB lensing is directly proportional to the overlap of their kernels. The cosmic infrared background and 21 cm surveys probe the high redshift structures and, independent of the model assumed, they show a relatively good overlap with the CMB lensing kernel. On the other end, galaxy clustering surveys can only reconstruct the low- $z$  portion of the lensing kernel as can be seen from the LSST, DES and DESI curves. However, given the low noise of these measurements and their small overlap with other probes, they can still play a major role in delensing even if their overlap with the CMB lensing potential is not optimal.

### 3.0.3 Improving efficiency with tomographic binning

The delensing efficiency of galaxy surveys can be improved by taking into account redshift information. When we weight a tracer with  $\frac{C^{\kappa I}}{C^{II}}$  in Eq. (3.8) in order to maximize its ability to reconstruct the lensing potential we are only using redshift averaged information about the survey. However, as can be seen in Fig. 3.2, the kernel overlap of a tracer with the CMB lensing varies as a function of redshift. For this reason, the optimal approach is to weight galaxies at different redshift with different weights according to both their cross-correlation with  $\kappa$  and their auto-spectrum. We can see this with a simple example. Let's split a single survey  $I$  into two non-overlapping redshift bins  $I_1$  and  $I_2$  with  $I = I_1 + I_2$ . For the full survey the effective cross-correlation is equal to

$$\rho_{\text{full}}^2 = \frac{(C_l^{\kappa I})^2}{C_l^{\kappa\kappa} C_l^{II}} = \frac{(C_l^{\kappa I_1} + C_l^{\kappa I_2})^2}{C_l^{\kappa\kappa} (C_l^{I_1 I_1} + C_l^{I_2 I_2})} \quad (3.13)$$

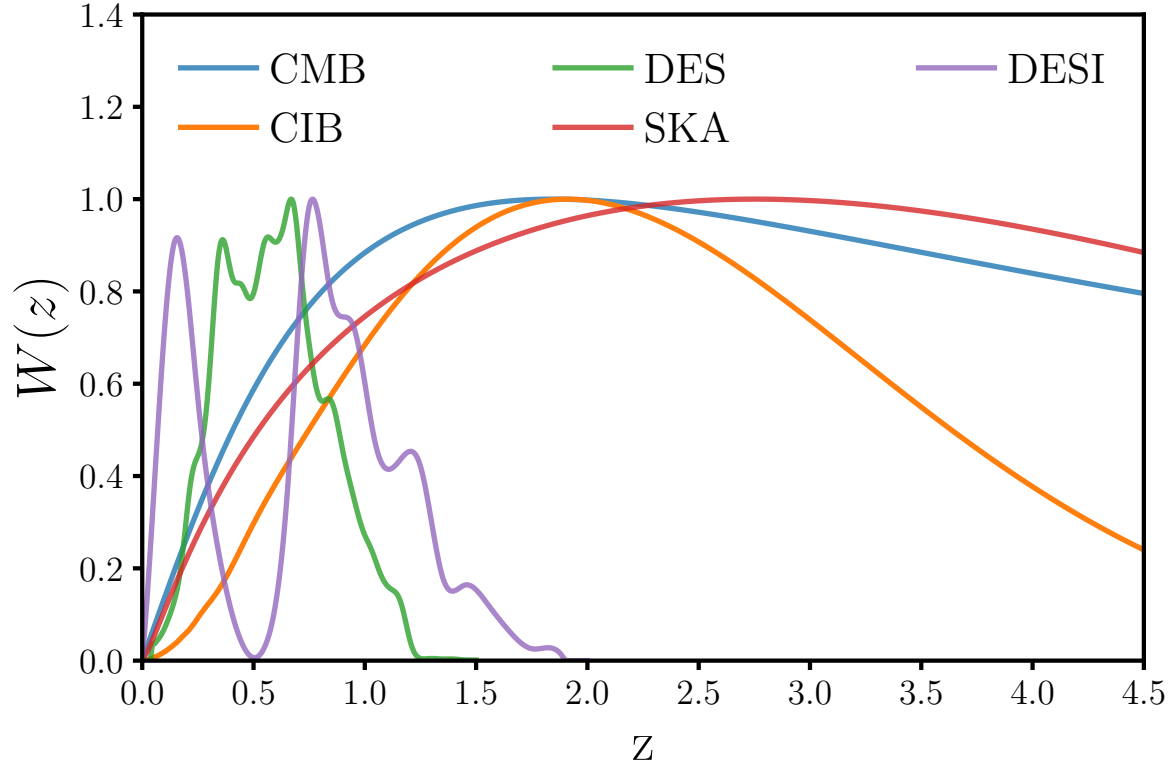


Figure 3.2: Kernel Comparison: Comparison of the different kernels as a function of redshift for some of the tracers used in this analysis. The bigger the overlap with the CMB lensing kernel the better the reconstruction of the lensing potential is thus leading to a higher delensing efficiency.

while for the split survey it will be

$$\rho_{\text{split}}^2 = \frac{(C_l^{\kappa I_1})^2}{C_l^{\kappa\kappa} C_l^{I_1 I_1}} + \frac{(C_l^{\kappa I_2})^2}{C_l^{\kappa\kappa} C_l^{I_2 I_2}}. \quad (3.14)$$

Now it can be show that  $\rho_{\text{split}} \geq \rho_{\text{full}}$  since:

$$\rho_{\text{split}}^2 - \rho_{\text{full}}^2 \propto (C_l^{I_1 I_1} C_l^{\kappa I_2} - C_l^{I_2 I_2} C_l^{\kappa I_1})^2 \quad (3.15)$$

Then  $\rho^2$  is always larger in the tomographic case, and the two are equal only when  $\frac{C_l^{\kappa I_i}}{C_l^{I_i I_i}}$  is the same for all the redshift bins in which case a single optimal weight is sufficient for the entire survey. Binning will improve the efficiency of galaxy surveys, but it is not very effective for tracers with poor redshift information like the CIB or radio continuum surveys.

In this work, we bin both photometric and spectroscopic galaxy surveys by splitting the window function Eq. (2.5) into different slices such as all the bins contain the same number of galaxies. For photometric surveys like DES and LSST, we assume a photometric redshift estimation gaussianly distributed around the true value with an rms fluctuation  $\sigma(z)$ .

In that case the  $i^{\text{th}}$  slice has a galaxy distribution [14]:

$$W_i(z) \propto b(z) \frac{dN(z)}{dz} \left[ \text{erfc} \left( \Delta(i-1) - z \frac{\sigma(z)}{\sqrt{2}} \right) - \text{erfc} \left( \Delta i - \frac{z}{\sigma(z)} \sqrt{2} \right) \right]. \quad (3.16)$$

For photometric surveys, the maximum number of bins is dictated by the fact that the bin width can not be smaller than the photo-z accuracy. We used 10 and 4 photometric bins for LSST and DES respectively with a photo-z accuracy of  $\sigma(z)_{\text{DES}} = 0.05(1+z)$  for DES and  $\sigma(z)_{\text{LSST}} = 0.01(1+z)$  for LSST. In spectroscopic surveys, there are no limitations in increasing the number of bins. We split DESI into 4 spectroscopic bins with no overlap among each others. This number of bins is close to the saturation point where adding more

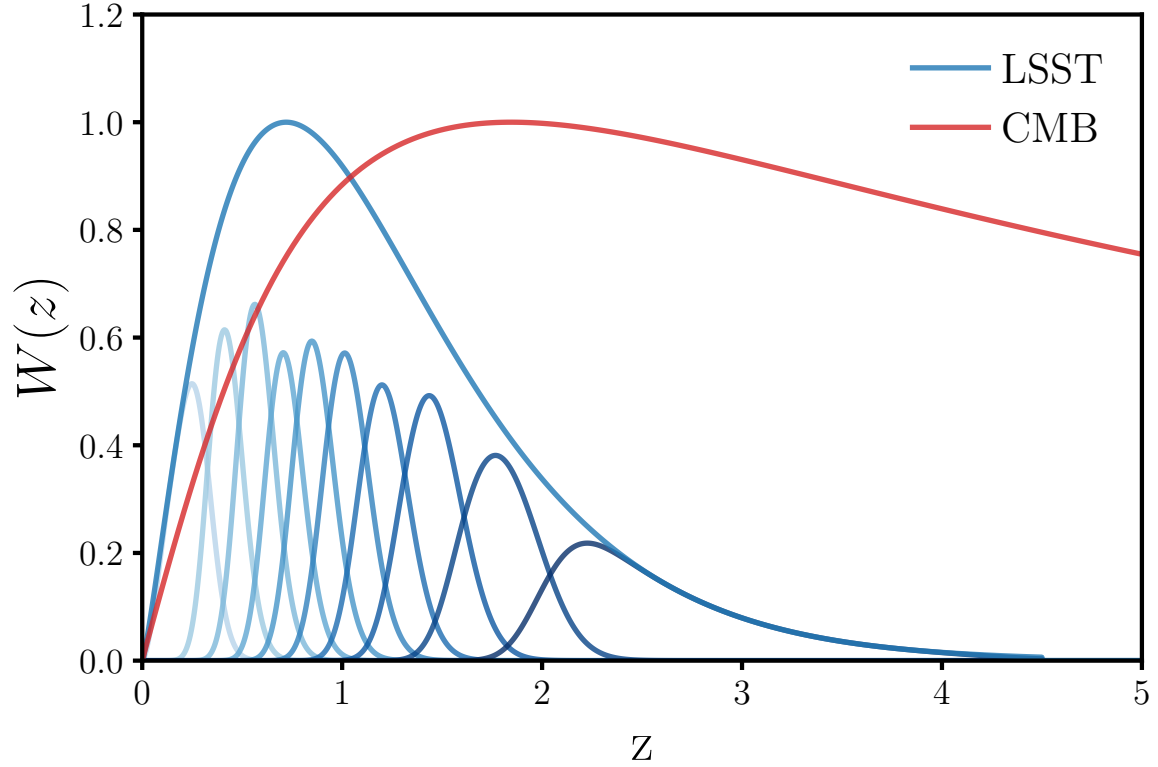


Figure 3.3: Comparison of kernels of the 10 LSST tomographic bins together with the full LSST survey and the CMB lensing kernel. Compared to a full survey approach, tomographic binning allows to optimally weight different bins according to their cross-correlation with the CMB lensing. This leads to a better delensing efficiency.

bins does not improve delensing significantly while adding complexity to the analysis. As an example, we show in Fig. 3.3 the 10 bins and the full LSST redshift distributions together with the CMB lensing kernel. Fig. 3.4 illustrate the improvement obtained by tomographic binning. In particular on large scales, binning can increase the value of  $\rho$  by almost 30% significantly improving the delensing efficiency of galaxy surveys.

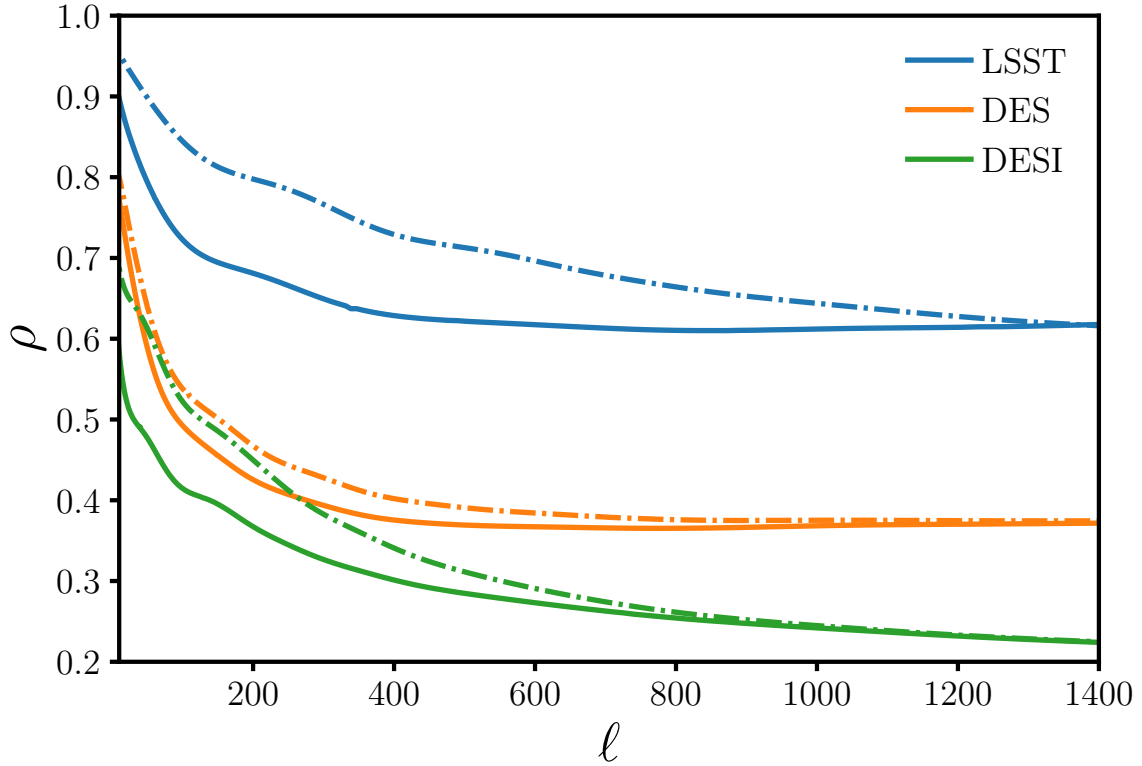


Figure 3.4: Tomographic bins improve the cross-correlation of galaxy surveys with CMB lensing. Here we show the cross-correlation coefficient (Eq. (3.10)) as a function of angular scale for full surveys (solid lines) and tomographically binned surveys (dot-dashed line).

For details about the binning, see section 3.0.3 and in particular Eq. (3.16).

# CHAPTER 4

## PARAMETER CONSTRAINTS IMPROVEMENT AFTER DELENSING

In this section, we forecast the expected delensing efficiency and the relative importance of galaxy tracers for delensing in current and future experiments. We will use the Fisher information matrix to quantify the delensing efficiency as the improvement in the constraint of two inflationary parameters: the tensor to scalar ratio  $r$  and the tensor tilt  $n_T$ . We assume a CMB experimental scenario composed of a high-resolution CMB experiment which defines the ability to internally reconstruct the potential  $\kappa$ , together with a low-noise, low-resolution experiment that measured the B-modes that will be delensed and used to constrain the inflationary parameters. Even if there is not a definite distinction between different stages, we focus on three distinct scenarios: the current stage, a third generation stage (3G) and finally the futuristic CMB Stage 4.

### *4.0.1 Fisher Information Matrix*

In the Fisher Information Matrix formalism [10], the statistical uncertainty on a cosmological parameter  $p$  can be obtained from the inverse of the Fisher matrix  $F_{ij}$  as  $\sigma(p) = \sqrt{(\mathbf{F})_{pp}^{-1}}$ . We constrain the inflationary parameters  $p = \{r, n_t\}$  with a CMB B-mode spectrum measurement so the Fisher matrix is:

$$F_{ij} = \sum_{\ell=\ell_{min}}^{\ell_{max}} \frac{1}{\sigma(C_\ell^{BB})^2} \frac{\partial C_\ell^{BB}}{\partial p_i} \frac{\partial C_\ell^{BB}}{\partial p_j} \quad (4.1)$$

where we assume a Gaussian covariance:

$$\sigma(C_\ell^{BB}) = \sqrt{\frac{2}{(2\ell+1)f_{\text{sky}}}} \left( C_\ell^{BB,r} + C_\ell^{BB,\text{lens}} + N_\ell^{BB} \right). \quad (4.2)$$

The B-modes noise spectrum is given by [19]:

$$N_\ell^{BB} = (\Delta_P/T_{\text{CMB}})^2 e^{l^2 \theta_{\text{FWHM}}^2 / (8 \ln 2)} \quad (4.3)$$

where  $\theta_{\text{FWHM}}$  is the full half width of the telescope beam, and  $\Delta_P$  is the instrumental noise of the experiment.

It can be seen in Eq. (4.1) that removing the lensing contribution will improve parameter constraints. The parameter uncertainties are inversely proportional to the covariance of the measurement. Since the lensing B-modes power  $C_l^{BB,\text{lens}}$  is a substantial component of the covariance, removing part of it through delensing will reduce the parameter statistical error. We define the error after delensing as  $\sigma^{\text{del}}(p)$ . This is computed from Eq. (4.1) substituting  $C_l^{BB,\text{lens}}$  with the residual power after delensing  $C_l^{BB,\text{res}}$  in the covariance matrix defined in Eq. (4.2). We define the improvement as the ratio of the constraints before and after delensing:  $\alpha_r = \sigma^{\text{del}}(r)/\sigma(r)$  and  $\alpha_{n_t} = \sigma^{\text{del}}(n_t)/\sigma(n_t)$ . The fiducial values used are described in section 4.0.2. Given a fiducial value for  $r$ , the value of  $n_t$  is fixed imposing the consistency relation  $n_t = -r/8$  [23].

In Eq. (4.1) we are making a few important assumptions. First, we are fixing all the cosmological parameters except  $\{r, n_t\}$ . Uncertainties in those will propagate to larger uncertainties in  $\{r, n_t\}$ . While neglecting this will lead to slightly optimistic constraints, it has no significant impact on the estimate of the improvement due to delensing.

We are also neglecting an important contribution to the measured CMB B-modes: galactic polarized foregrounds. The amplitude of these has been constrained in [6, 30] and it strongly varies in different parts of the sky. Future experiments will use multi-band data to exploit the frequency dependence of these contaminants to remove them from the data. The amount of residual foregrounds depends both on uncertain foreground properties and experimental choices (see a review in [1]). For this reason, accurately treating foreground requires the use of simulations and the knowledge of several experimental details. We de-

cided to focus on an ideal situation assuming no foregrounds or perfect cleaning even if the importance of delensing will be slightly overestimated.

Furthermore, we are not considering the uncertainties on galaxy survey internal parameters such as biases, source distributions and photometric redshift uncertainties. These uncertainties can significantly degrade inflationary constraints [41, 29]. However, as shown in [41, 29], these can be auto-calibrated i.e. they can be tightly constrained using galaxy survey auto- and cross-correlation spectra. We checked this for a few of the tracer combinations used here and find it particularly true once several tracers are jointly taken into account. Finally, although we have assumed a Gaussian covariance  $\sigma(C_\ell^{BB})$  it actually has small non-Gaussian contributions [27, 3]. This approximation is good enough to show the improvement due to delensing. The approximations made here go in the direction of a slightly optimistic *absolute* value for the parameters statistical uncertainties both for the standard and the delensed case. The delensing improvement is defined as the *relative* value of these uncertainties  $\alpha_i = \sigma^{\text{del}}(i)/\sigma(i)$  and, at first order, it is not affected by this assumptions.

#### 4.0.2 Delensing with current CMB and LSS

Recently delensing has been performed for the first time on data using both CIB maps [21, 26] and internal CMB lensing maps [7] as large scale structure tracers. Here we discuss the improvement that can be obtained by combining these and other currently Stage-2 available tracers (see [48] for publicly accessible multi-tracers data-products).

On the CMB side, we will combine a BICEP-Keck like *deep* CMB experiment with an overlapping *higher resolution* experiment. For the deep experiment we assume an instrumental noise equal to  $3\mu\text{K-arcmin}$ , a beam of 30 arcmin and an angular scale range of  $50 < \ell < 500$ . We assume the CMB lensing reconstruction is performed by the higher resolution CMB experiment. We explore two possibilities. First, we test the delensing efficiency with an internal reconstruction of CMB lensing performed by the Planck collaboration [32].

We compute the noise in the CMB lensing map in Eq. (2.4) using the noise curves publicly available <sup>1</sup>. Then, we test a second scenario with a ground-based experiment characterized by noise levels consistent with SPT-Pol:  $9.4\mu\text{K-arcmin}$  in polarization with a beam equal to  $1.2\text{ arcmin}$ . In this case we set the largest achievable scale at  $\ell_{min} = 300$ . However, the results are robust against this choice since the neglected scales contribute only moderately to the reconstruction of the CMB lensing potential.

We combine these CMB experiments with the CIB and current low redshift galaxy surveys like DES and WISE and we compute the improvement in the delensing efficiency. Following [48] we cut both the CIB and WISE at  $\ell < 100$  where they are contaminated by large Galactic dust residuals. Optical surveys galaxies like DES are less affected by dust and can be used on larger scales. The achievable correlation is shown in Fig. 4.1 for Planck and in Fig. 4.2 for SPT-Pol. In these figures we include a dashed curve that corresponds to (with arbitrary scale)  $< C_{\ell}^{\kappa\kappa} \times \frac{\partial C_{\ell'}^{BB}}{\partial C_{\ell}^{\kappa\kappa}} >_{\ell' < 100}$ , in order to show which scales in  $\kappa$  contribute to the  $\ell < 100$  B-mode power.

For Planck, the internal reconstruction is at most 70% correlated at very large scales and then it falls rapidly to 40% at  $\ell = 200$ . Its correlation is comparable to the one of LSS at almost all scales. On the other end, the CMB lensing reconstruction from SPT-Pol will be more than 80% correlated with the true field at  $\ell < 300$ , and only then the correlation becomes comparable to the current LSS surveys. In both cases the CMB lensing reconstruction correlates very well at low  $\ell$  and it then falls rapidly at smaller scales because of the raise of the reconstruction noise.

Fig. 4.2 and Fig. 4.1 show that the DES galaxies are effective tracers of the LSS and can, at least in the near future, be used to improve delensing for CMB experiments that overlap with it. For example, DES delensing efficiency is higher than WISE first because of the lower level of noise and also because DES galaxies are located at slightly higher redshift so

---

1. [https://wiki.cosmos.esa.int/planckpla2015/index.php/Specially\\_processed\\_maps](https://wiki.cosmos.esa.int/planckpla2015/index.php/Specially_processed_maps)

they better overlap with CMB lensing. As expected the improvement of the internal CMB reconstruction reduces the relative importance of LSS. In particular it can be seen in Fig. 4.2 that optical surveys will rapidly lose the role of filling in large-scale modes and they will start to supplement information at higher multipoles.

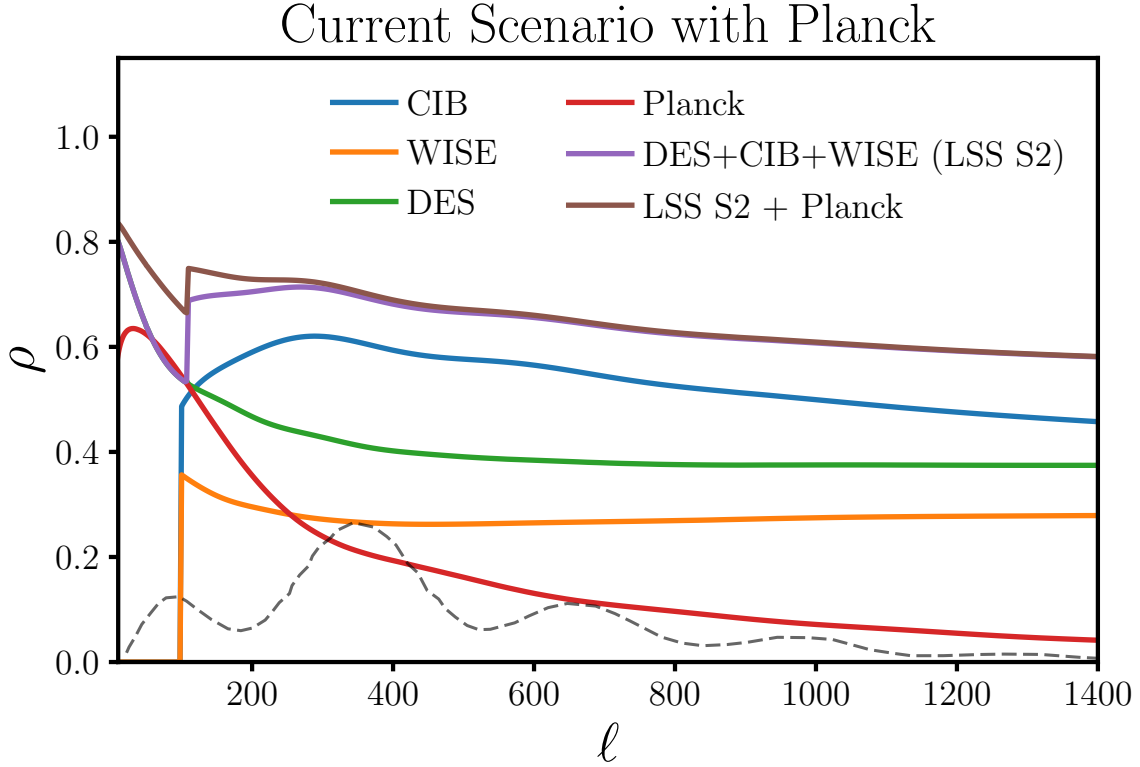


Figure 4.1: Correlation factor  $\rho$  with the CMB lensing potential as a function of the angular scale  $\ell$  for completed and ongoing Stage-2 tracers. Here we show both current galaxy survey and internally reconstructed CMB lensing potential. The dashed curve highlights which scales contribute to the  $\ell < 100$  B-mode power and are thus most useful to delens. It corresponds to (with arbitrary scale)  $C^{\kappa\kappa} \times \frac{\partial C^{BB}}{\partial C^{\kappa\kappa}}$

Using these correlation levels we can compute the residual B-mode power after delensing using Eq. (3.9), and test the consequent improvement on parameter constraints with Eq. (4.1). For current surveys we only consider  $p = r$  since the broad beam of the deep BK-like survey does not provide enough leverage to constrain the shape of the B-mode spectra.

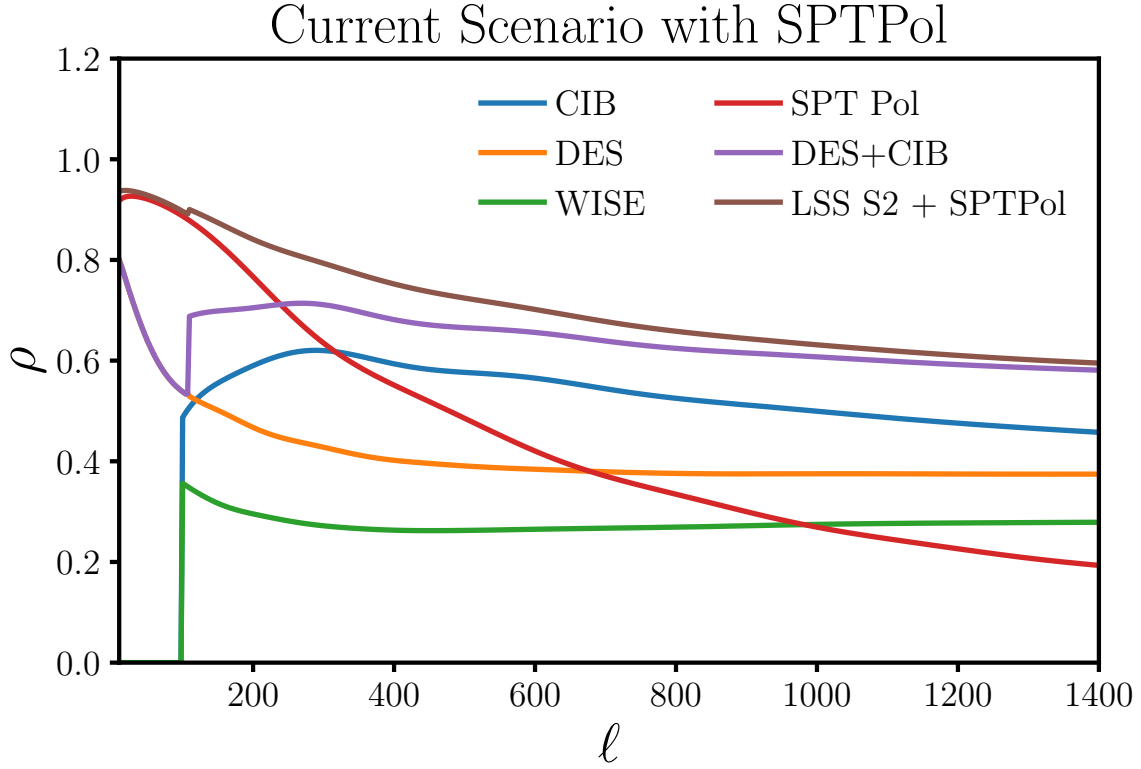


Figure 4.2: Correlation factor  $\rho$  with the CMB lensing potential as a function of the angular scale  $\ell$  for completed and ongoing Stage-2 tracers. This figure is the same as Fig. 4.1 but using SPTPol instead of Planck as the high-res CMB experiment performing the internal reconstruction.

We still let  $n_t$  to vary in our fisher calculation even if it is not very degenerate with  $r$ . We first compute the improvement with a fiducial value of  $r_{\text{fid}} = 0$ . The results are summarized in Tab. 4.1 and Tab. 4.2 for the Planck and SPTPol case respectively.

The lensing reconstruction noise in Planck is such that internal delensing can only remove 8% of the power, improving the constraints on  $r$  by a factor of 1.06 even in the ideal scenario of no instrumental noise in the B-modes. A similar performance is achieved with WISE. DES can do better, removing a level of 14% of power. However, it covers a smaller fraction of the sky than the two previous probes. As shown in previous works [41], the best tracer is the CIB with a 27% reduction in power. Nonetheless, it is worthwhile combining all the tracers. Indeed a multi tracer-approach can bring the removed power on the overlapping area from 27% of the CIB alone to 36% using all the LSS (LSS-S2) and 41% when Planck lensing reconstruction is added to the set. However, if we consider a realistic level of noise in the measured B-modes, this level of residual power  $C_l^{BB,\text{res}}$  only leads to a 30% improvement in  $\sigma(r)$  for the null hypothesis case of  $r = 0$ . Furthermore, as explained in section 4.0.1, this is only an upper limit and will be even smaller when, for example, non-perfect foreground cleaning is considered. Indeed current experiments are still significantly limited by foregrounds and instrumental noise together and not only by lensing.

If, on the other hand, we consider a high-resolution ground base experiment the internal lensing reconstruction improves significantly. Tab. 4.2 shows that, with an instrumental noise at the expected level for SPTPol, the CMB will soon be able to remove an amount of power (35%) at the level of the CIB. Once combined with LSS tracer this will lead to removing 56% of the power. The improvement of 1.57 in  $\sigma(r)$  that will follow, even when realistic noise is considered, is such that it will make delensing a needed step for CMB polarization data analysis.

We also test a scenario where primordial gravitational waves are present at their highest possible value of  $r_{\text{fid}} = 0.12$  [6]. As expected the importance of delensing itself is now reduced

Table 4.1:  $\alpha(r)$ : Improvements on  $\sigma(r)$  due to delensing for completed and ongoing Stage-2 surveys and Planck lensing reconstruction. LSS-S2 corresponds to the combination of all the available LSS tracers. The values in parenthesis in the first column correspond to the fraction of lensing B-mode power removed using each LSS tracer. The values in the other columns correspond to ratio of the error before and after delensing for 3 cases: no instrumental noise in the B-mode measurement and realistic noise for two different values of  $r$ .

Surveys	$\alpha_{r=0}, N_{\ell}^B = 0$	$\alpha_{r=0}$	$\alpha_{r=0.12}$
WISE (6%)	1.09	1.05	1.01
DES (14%)	1.2	1.10	1.03
CIB (27%)	1.45	1.21	1.07
LSS-S2 (36%)	1.7	1.29	1.09
CMB Planck (8%)	1.06	1.05	1.01
LSS-S2 +CMB (41%)	1.77	1.31	1.10

Table 4.2:  $\alpha(r)$ : Stage-2 improvements on  $\sigma(r)$  due to delensing. We use the same LSS tracers as Tab. 4.1 but with the internal lensing reconstruction performed by SPTPol.

Surveys	$\alpha_{r=0}, N_{\ell}^B = 0$	$\alpha_{r=0}$	$\alpha_{r=0.12}$
SPTPol (35%)	1.46	1.27	1.08
LSS-S2 +SPTPol (56%)	2.18	1.57	1.16

given that the lensing component constitutes a smaller portion of the total B-modes variance

### 4.0.3 CMB-S3 Era

CMB polarization measurements are rapidly improving. Indeed the next generation of ground-based telescopes has been already deployed, and data are currently being taken. As we did for Stage-2, we model the CMB S3 as two different overlapping experiments that will be able to combine their measurement. The two experiments combined will have a level of noise of  $3\mu\text{K-arcmin}$  and a 1 arcmin beam. This level of noise is also assumed for the internal noise reconstruction. With this experimental setup, we can push the angular scale range used to calculate the Fisher matrix to  $50 < \ell < 3000$  even if most of the high  $\ell$  scale do not contribute to the constraints. Not only will CMB experiments improve shortly: eventually DESI will start taking data. For this reason, we add DESI to the LSS tracers used in

section 4.0.2.

The correlation factor attainable using generation 3 experiments is shown in Fig. 4.3. An interesting finding is that DESI will be less efficient (removing 10% of the power) than a DES-like survey (14%) despite the fact that it can probe slightly higher redshift. The reason is that, because of the broad CMB kernel, spectroscopic redshift accuracy is not needed and the lower shot noise in DES increases the delensing efficiency significantly. Unfortunately, adding DESI will only bring the power removed using LSS from 36 to 41%. Indeed, even in the near future, CIB will still play the dominant role among LSS. Contrary to current experiments, the CMB internal reconstruction will dominate the correlation with the lensing potential up to  $\ell \simeq 550$ .

We summarize the improvement in the constraint on  $r$  in Tab. 4.3. Given the improvement in the noise of the high-resolution experiment, CMB alone will be able to improve constraint on  $r$  by a factor of 2 through internal delensing in the ideal case of no instrumental noise. Adding galaxy surveys will lead to a further improvement without additional effort. Indeed galaxy surveys will still be able to remove an additional 20% of power from  $C_\ell^{BB,\text{lens}}$  and to improve our constraint on the null hypothesis ( $r = 0$ ) by 15%. Note that apart from the addition of DESI, the tracers used here are already available today. The ongoing effort can then lead to a significant improvement even for the next generation of experiments. Finally, the combination of CMB and galaxy surveys will be able to improve the constrain on the null hypothesis of no primordial waves by a factor 1.8 or to improve the constraint of a possible detection ( $r=0.12$ ) by 30%. As expected the improvement on  $n_t$  is similar to the one in  $r$  since they are both proportional to the variance of the measured B-modes. We tested this in the scenario  $r = 0.12$  where we additionally impose the consistency relation  $n_t^{\text{fid}} = -r^{\text{fid}}/8$ . It is important to note that, independent of the level of delensing, for CMB 3G experiments the statistical error on  $n_t$  will still be several times bigger than the fiducial value.

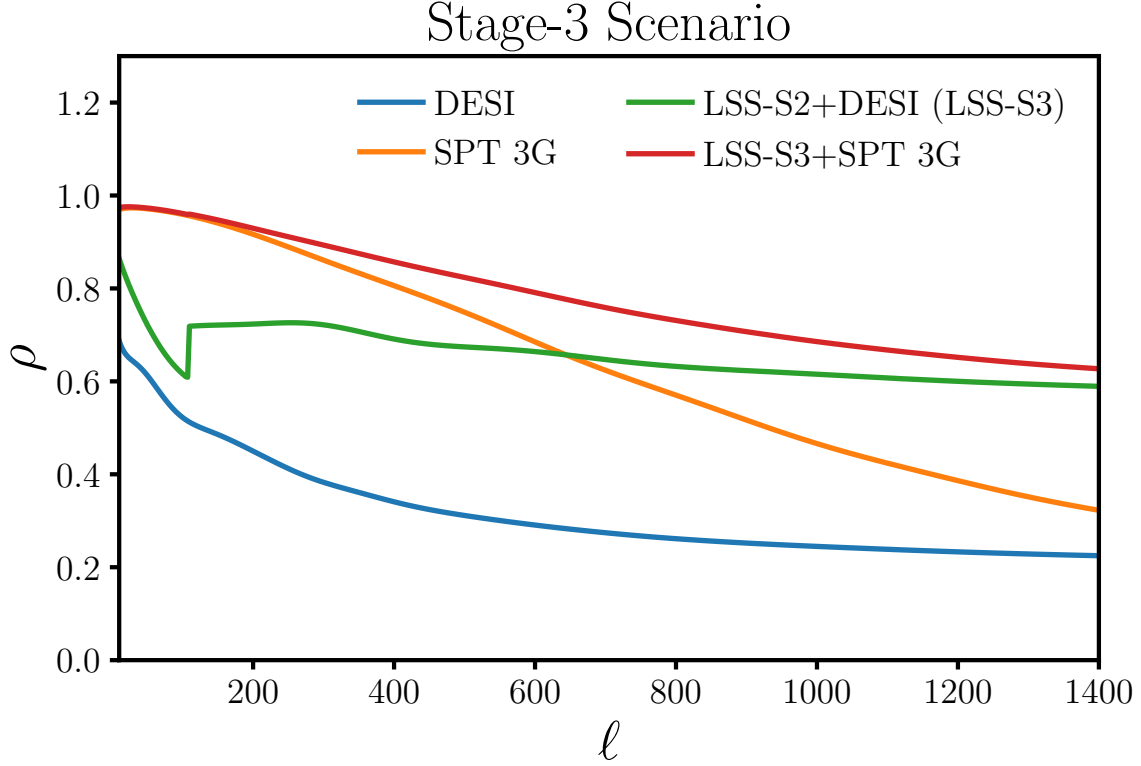


Figure 4.3: Correlation factor  $\rho$  with the CMB lensing potential as a function of the angular scale  $\ell$ . This figure is the same as Fig. 4.2 but with a stage-3 CMB experiment performing the internal reconstruction and with DESI added to the stage-2 galaxy surveys (LSS-S2).

Table 4.3:  $\alpha$ : Improvements on  $\sigma(r)$  due to delensing for S3 experiments. Here we define LSS-S3 as the combination of S2 LSS tracers (LSS-S2) and DESI. We also use a CMB S3 experiment for the lensing internal reconstruction. See section 4.0.3 for details.

Surveys	$\alpha_{r=0, N_\ell^B = 0}$	$\alpha_{r=0}$	$\alpha_{r=0.12}$
DESI (10%)	1.12	1.08	1.03
LSS-S3 (40%)	1.73	1.42	1.2
CMB 3G (56%)	2	1.57	1.21
LSS-S3+CMB (69%)	2.8	1.8	1.31

#### 4.0.4 CMB-S4 Era

Having as a major goal the detection of inflationary B-modes, CMB data will continue improving even after Stage-3. An ambitious program for a Stage-4 ground CMB experiment is in the planning phase [1]. Moreover, satellite and balloon CMB experiments have been proposed and have the potential to extend the accessible B-mode measurements to the largest scales. Given the unprecedented low level of noise of these experiment, delensing will be even more important than previous generations. Following [1], here we assume a CMB-S4 ground experiment with a level of noise of  $1\mu\text{K-arcmin}$  and a  $1\text{ arcmin}$  beam. Furthermore, by the mid-2020s, several next-generation LSS surveys will be online. Here, as an example of future optical galaxy surveys, we add LSST [25] to the CMB lensing tracers. We do not consider other surveys but we test that other experiments like Euclid [22] and WFIRST [44] have similar delensing performance. Even if these LSS surveys will observe an overlapping part of the sky and similar modes, because of their different strengths and weaknesses, it will still be important to combine them efficiently. We also consider a radio continuum survey modeled following the SKA specifications. Radio continuum observations of the 21 cm line are in their early stage, and several experimental and data-analysis challenges need to be overcome. However, this technique has the potential to map the LSS with relatively low noise up to redshift  $z = 6$ . Here we considered just two possible detection thresholds at 1 GHz (flux cut):  $10\text{ }\mu\text{Jy}$  and  $0.1\text{ }\mu\text{Jy}$ , which are representatives of the upper and lower limit levels for a SKA phase 1 (SKA1) and a following SKA phase 2 (SKA2) survey. Given the importance of delensing for Stage-4 experiments, here we combine radio and optical survey to test their delensing efficiency.

The correlation factor with CMB lensing for Stage-4 experiments is shown in Fig. 4.4 and in Fig. 4.5 for SKA1 and SKA2 respectively. A tomographically binned LSST-like experiment will be a very efficient CMB lensing tracer. Indeed it will be more than 70% correlated with CMB lensing for all the scales  $\ell < 600$ , a performance similar to a Stage-3 CMB internal

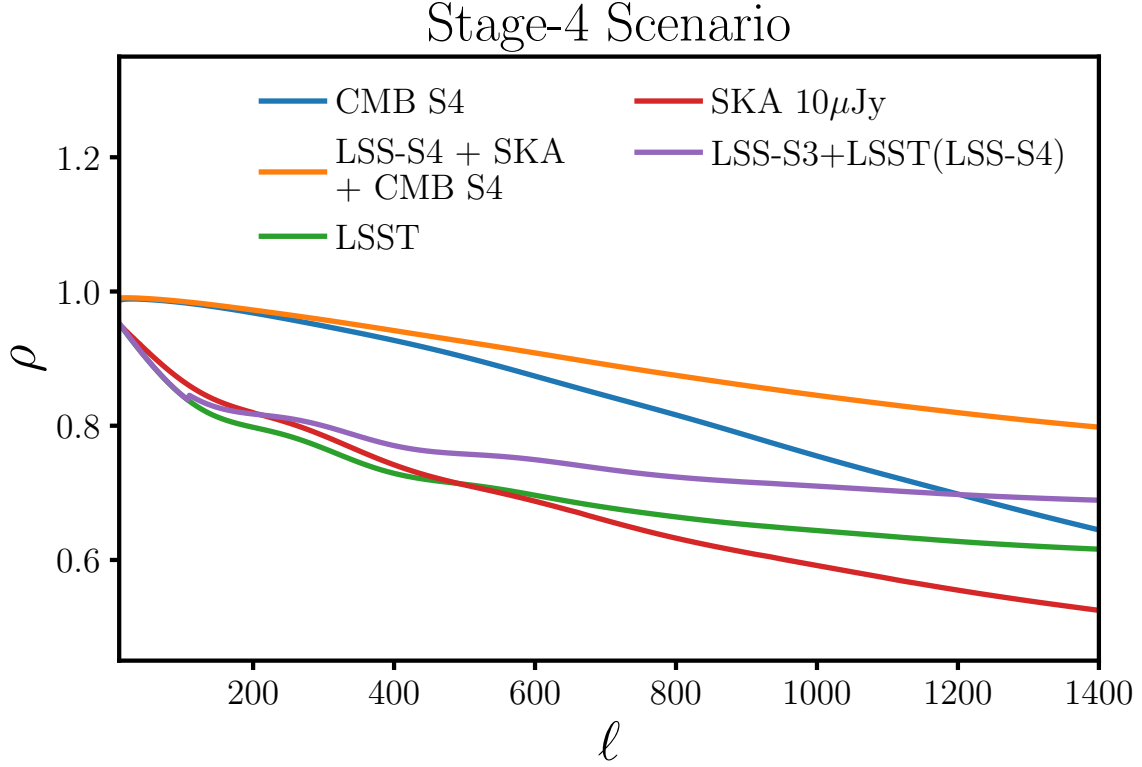


Figure 4.4: Correlation factor  $\rho$  with the CMB lensing potential as a function of the angular scale  $\ell$ . This figure is the same as Fig. 4.2 but with a stage-4 CMB experiment performing the internal reconstruction and with LSST and SKA added to the stage-2 and stage-3 galaxy surveys (LSS-S3).

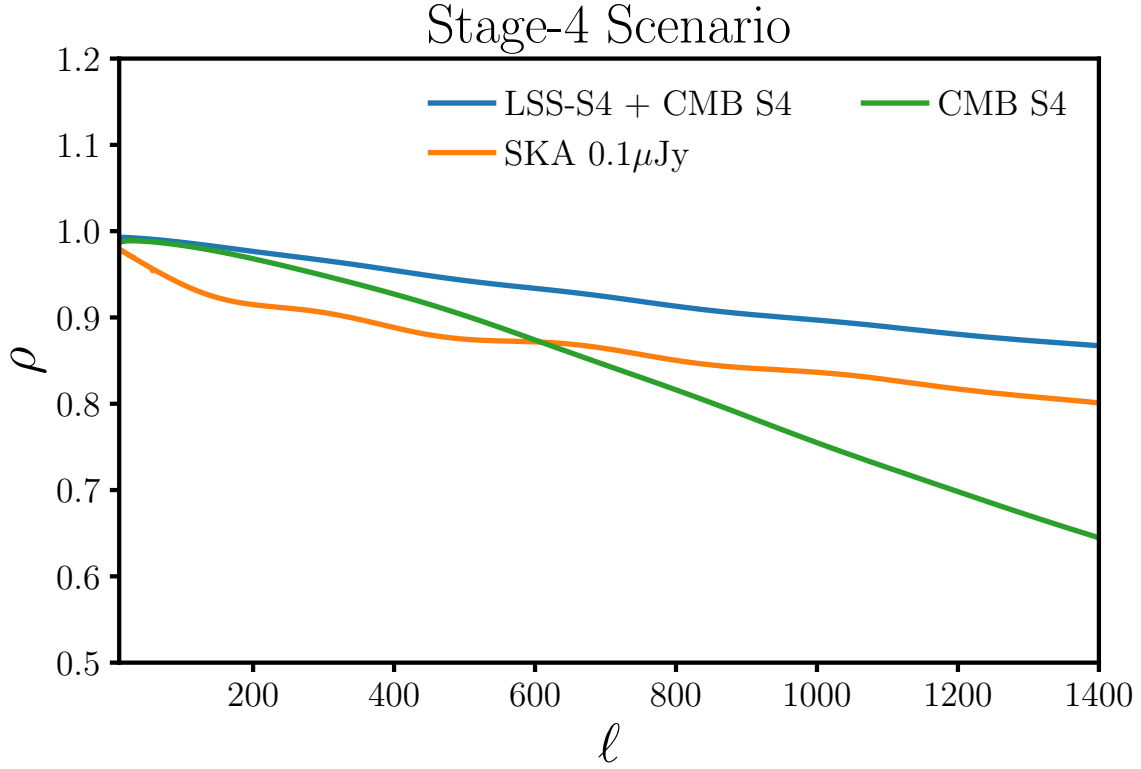


Figure 4.5: Correlation factor  $\rho$  with the CMB lensing potential as a function of the angular scale  $\ell$ . This figure is the same as Fig. 4.2 but with a stage-4 CMB experiment performing the internal reconstruction and with LSST and SKA added to the stage-2 and stage-3 galaxy surveys (LSS-S3).

reconstruction. A very similar level of efficiency will be achieved by a SKA1-like experiment. With SKA and LSST, for the first time we will have LSS tracers with a higher delensing efficiency than the CIB. Despite the improvement in galaxy surveys, the CMB internal reconstruction will still be the main source of delensing. Having a perfect kernel overlap with the true lensing potential it will benefit from the very low level of noise of CMB S4 experiments. Fig. 4.4 shows that a CMB-S4 experiment will be able to internally reconstruct the lensing potential at more than 90% up to  $\ell = 400$ . At this level, CMB S4 internal delensing will not be limited by noise but by small secondary effects like foregrounds contamination, filtered modes etc. Finally, Fig. 4.5 shows that a very futuristic SKA-2 experiment will have a very high correlation with CMB lensing, being more than 80% correlated at all the scales. This performance is comparable to a CMB-S4 internal reconstruction.

Tab. 4.4 shows the improvement on the inflationary constraint given the cross-correlation factors described above. LSST alone will be able to remove almost half of the B-mode lensing power. This will lead to an improvement in  $\sigma(r)$  of a factor of 1.8. If we add all the other infrared and optical LSS tracers previously included (i.e. excluding SKA) the improvement factor increase to 2.3. These gives an important opportunity: for sufficiently high values of  $r$  it will be possible to confirm a detection of primordial gravitational waves using spectra delensed with LSS, completely independent of CMB internal data. Similarly to [29] we find that SKA phase-1 radio survey will remove 53% of the lensing power and, once combined with optical and infrared surveys, this will allow the level of power removed using LSS (62%) to surpass the level of the CMB S3 internal reconstruction. Finally, as previously mentioned, CMB S4 will be the main source of delensing with the ability of removing up to more than 80% of the B-modes power. This will bring an almost factor of 4 improvement in the null test case even with realistic noise. Combining with LSS will only increase the removed power compared to CMB only by  $\simeq 5\%$  but it will be highly beneficial to test the robustness of the final result.

Table 4.4:  $\alpha$ : Improvements on  $\sigma(r)$  due to delensing for S4 experiments. Here we define LSS-S4 as the combination of S3 LSS tracers (LSS-S3) and LSST. We also consider SKA-like radio-continuum surveys. We also use a CMB S4 experiment for the lensing internal reconstruction. See section 4.0.4 for details.

Surveys	$\alpha_{r=0}, N_\ell^B = 0$	$\alpha_{r=0}$	$\alpha_{r=0.12}$
LSST (48%)	1.8	1.7	1.7
LSS-S4 (60%)	2.5	2.3	2.3
SKA ( $10\mu\text{Jy}$ ) (53%)	2.1	2	2
SKA ( $0.1\mu\text{Jy}$ ) (77%)	4.6	3.9	3.9
LSS-S4 + SKA ( $10\mu\text{Jy}$ ) (65%)	2.7	2.5	2.5
LSS-S4 + SKA ( $0.1\mu\text{Jy}$ ) (80%)	4.6	3.9	3.9
CMB S4 (81%)	5.1	4.3	4.2
LSS+CMB (86%)	5.2	4.4	4.3

We find the improvement in  $\sigma(n_t)$  to be very similar to the one in  $\sigma(r)$  for all the CMB-S4 cases. This is reasonable because, given the level of noise in CMB-S4, the variance at angular scales  $\ell < 200$  are dominated by instrumental noise and not by the lensing component. Independent of the delensing level, the small value allowed for  $r$  will not allow to test the consistency relations.

## CHAPTER 5

### CONCLUSIONS

The ability to separate the lensing component of the CMB B-modes from a possible primordial inflationary signal (“delensing”) is necessary to test inflation using the next generation of CMB polarization experiments. To delens, we need to accurately reconstruct the large scale structures that lens the CMB in order to build a template of the expected lensing B-modes in the observed patch. In this paper, we studied the potential impact of large-scale structure galaxy surveys in this important endeavor.

For ongoing experiments, we find that LSS tracers will be particularly beneficial. An optical survey like DES is able to remove 14% of the B-mode lensing power alone, and together with WISE(8%) and the CIB (27%) will allow to remove 36% of the power using only LSS surveys. Depending on the CMB instrumental noise and the amount of galactic foreground cleaning, delensing using LSS survey can correspond to a maximum improvement of 30% in the constraint on the tensor to scalar ratio  $r$  compared to the value before delensing. In the future, the decreasing level of instrumental noise in CMB experiments will dramatically improve the internal reconstruction of the structures lensing the CMB. The fraction of removed lensing B-modes will rapidly improve from the current expected levels for Planck (8%) and SPTPol (35%) to 3G (56%) and CMB S4 (85%) levels. For Stage-3 experiments, the CMB internal reconstruction will be the main source of delensing. However, it will still be less efficient than galaxies at tracing the lensing potential at small scales  $\ell > 500$ . For this reason, combining galaxy survey with the CMB will push the fraction of removed power from 57% to 68% for 3G. Even for CMB S4, galaxy surveys will still play an important role. For example, a tomographically binned LSST-like survey by itself will remove 56% of the lensing power. This performance is lower than a S4 CMB internal reconstruction and comparable to a Stage-3 CMB. However, it will allow us to probe the robustness against systematics of an eventual detection of primordial gravitational waves. Indeed delensing with just CMB

data will require a careful study of possible biases and systematic effects because we delens the same dataset (the CMB) that we also use to reconstruct the lensing potential [7, 37, 28]. For this reason, efficient galaxies tracers are not only useful in the short term but, in the future, will also play a role in testing internal biases and performing consistency tests.

Given the high level of correlation of future galaxy surveys and CMB lensing, it is also worth looking for potential application besides the detection of inflationary B-modes. For example, delensing with galaxy surveys allows us to selectively remove from the CMB only the gravitational effect coming from the non-linear structures in the low-redshift universe. Removing this component will reduce the level of non-linearities both in the CMB and in the CMB lensing power spectrum providing an alternative route to exploit all the measurable modes without having to model the non-linear component at small angular scales.

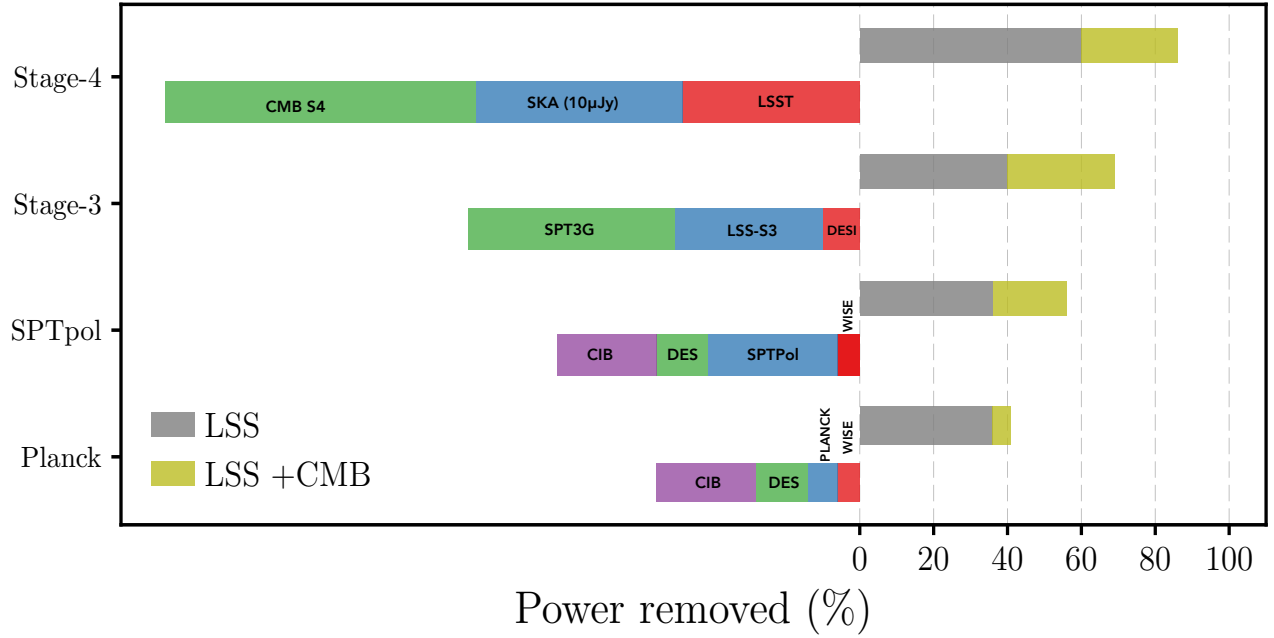


Figure 5.1: Summary of the amount of lensing B-modes power removed by different tracers for different generations of experiments. The bars on the left represent the individual contribution of different galaxy tracers. On the right, the gray bar represents the contribution from LSS only and the yellow one the total removed power once LSS and CMB internal reconstruction are combined. The values are taken from Tab. 4.1, Tab. 4.2, Tab. 4.3 and Tab. 4.4.

## CHAPTER 6

### ACKNOWLEDGMENTS

We thank S. Dodelson, S. Passaglia, K. Story, A. Vieregg and K. Wu for useful discussion and their review of the draft. Furthermore we thank D. Alonso for his feedback on radio continuum surveys.

This work made use of computing resources and support provided by the Research Computing Center at the University of Chicago. This work was partially supported by the Kavli Institute for Cosmological Physics at the University of Chicago through grants NSF PHY-1125897 and an endowment from the Kavli Foundation and its founder Fred Kavli.

## REFERENCES

- [1] K. N. Abazajian, P. Adshead, Z. Ahmed, S. W. Allen, D. Alonso, K. S. Arnold, C. Baccigalupi, J. G. Bartlett, N. Battaglia, B. A. Benson, C. A. Bischoff, J. Borrill, V. Buza, E. Calabrese, R. Caldwell, J. E. Carlstrom, C. L. Chang, T. M. Crawford, F.-Y. Cyr-Racine, F. De Bernardis, T. de Haan, S. di Serego Alighieri, J. Dunkley, C. Dvorkin, J. Errard, G. Fabbian, S. Feeney, S. Ferraro, J. P. Filippini, R. Flauger, G. M. Fuller, V. Gluscevic, D. Green, D. Grin, E. Grohs, J. W. Henning, J. C. Hill, R. Hlozek, G. Holder, W. Holzzapfel, W. Hu, K. M. Huffenberger, R. Keskitalo, L. Knox, A. Kosowsky, J. Kovac, E. D. Kovetz, C.-L. Kuo, A. Kusaka, M. Le Jeune, A. T. Lee, M. Lilley, M. Loverde, M. S. Madhavacheril, A. Mantz, D. J. E. Marsh, J. McMahon, P. D. Meerburg, J. Meyers, A. D. Miller, J. B. Munoz, H. N. Nguyen, M. D. Niemack, M. Peloso, J. Peloton, L. Pogosian, C. Pryke, M. Raveri, C. L. Reichardt, G. Rocha, A. Rotti, E. Schaan, M. M. Schmittfull, D. Scott, N. Sehgal, S. Shandera, B. D. Sherwin, T. L. Smith, L. Sorbo, G. D. Starkman, K. T. Story, A. van Engelen, J. D. Vieira, S. Watson, N. Whitehorn, and W. L. Kimmy Wu. CMB-S4 Science Book, First Edition. *ArXiv e-prints*, October 2016.
- [2] Graeme E. Addison, Joanna Dunkley, Amir Hajian, Marco Viero, J. Richard Bond, et al. Power-Law Template for IR Point Source Clustering. *Astrophys.J.*, 752:120, 2012.
- [3] A. Benoit-Lévy, K. M. Smith, and W. Hu. Non-Gaussian structure of the lensed CMB power spectra covariance matrix. *Phys. Rev. D*, 86(12):123008, December 2012.
- [4] BICEP2 Collaboration. Detection of B-Mode Polarization at Degree Angular Scales by BICEP2. *Physical Review Letters*, 112(24):241101, June 2014.
- [5] BICEP2 Collaboration, Keck Array Collaboration, P. A. R. Ade, Z. Ahmed, R. W. Aikin, K. D. Alexander, D. Barkats, S. J. Benton, C. A. Bischoff, J. J. Bock, R. Bowens-Rubin, J. A. Brevik, I. Buder, E. Bullock, V. Buza, J. Connors, B. P. Crill, L. Duband, C. Dvorkin, J. P. Filippini, S. Fliescher, J. Grayson, M. Halpern, S. Harrison, S. R. Hildebrandt, G. C. Hilton, H. Hui, K. D. Irwin, J. Kang, K. S. Karkare, E. Karpel, J. P. Kaufman, B. G. Keating, S. Kefeli, S. A. Kernasovskiy, J. M. Kovac, C. L. Kuo, E. M. Leitch, M. Lueker, K. G. Megerian, T. Namikawa, C. B. Netterfield, H. T. Nguyen, R. O’Brien, R. W. Ogburn, IV, A. Orlando, C. Pryke, S. Richter, R. Schwarz, C. D. Sheehy, Z. K. Staniszewski, B. Steinbach, R. V. Sudiwala, G. P. Teply, K. L. Thompson, J. E. Tolan, C. Tucker, A. D. Turner, A. G. Vieregge, A. C. Weber, D. V. Wiebe, J. Willmert, C. L. Wong, W. L. K. Wu, and K. W. Yoon. BICEP2/Keck Array VIII: Measurement of Gravitational Lensing from Large-scale B-mode Polarization. *ApJ*, 833:228, December 2016.
- [6] BICEP2/Keck Collaboration, Planck Collaboration, P. A. R. Ade, N. Aghanim, Z. Ahmed, R. W. Aikin, K. D. Alexander, M. Arnaud, J. Aumont, C. Baccigalupi, and et al. Joint Analysis of BICEP2/Keck Array and Planck Data. *Physical Review Letters*, 114(10):101301, March 2015.

- [7] J. Carron, A. Lewis, and A. Challinor. Internal delensing of Planck CMB temperature and polarization. *J. Cosmology Astropart. Phys.*, 5:035, May 2017.
- [8] H. Dole, G. Lagache, J.-L. Puget, K. I. Caputi, N. Fernández-Conde, E. Le Floc’h, C. Papovich, P. G. Pérez-González, G. H. Rieke, and M. Blaylock. The cosmic infrared background resolved by Spitzer. Contributions of mid-infrared galaxies to the far-infrared background. *A&A*, 451:417–429, May 2006.
- [9] S. Ferraro, B. D. Sherwin, and D. N. Spergel. WISE measurement of the integrated Sachs-Wolfe effect. *Phys. Rev. D*, 91(8):083533, April 2015.
- [10] R. A. Fisher. The logic of inductive inference. *Journal of the Royal Statistical Society*, 98(1):39–82, 1935.
- [11] N. R. Hall, R. Keisler, L. Knox, C. L. Reichardt, P. A. R. Ade, K. A. Aird, B. A. Benson, L. E. Bleem, J. E. Carlstrom, C. L. Chang, H.-M. Cho, T. M. Crawford, A. T. Crites, T. de Haan, M. A. Dobbs, E. M. George, N. W. Halverson, G. P. Holder, W. L. Holzapfel, J. D. Hrubes, M. Joy, A. T. Lee, E. M. Leitch, M. Lueker, J. J. McMahon, J. Mehl, S. S. Meyer, J. J. Mohr, T. E. Montroy, S. Padin, T. Plagge, C. Pryke, J. E. Ruhl, K. K. Schaffer, L. Shaw, E. Shirokoff, H. G. Spieler, B. Stalder, Z. Staniszewski, A. A. Stark, E. R. Switzer, K. Vanderlinde, J. D. Vieira, R. Williamson, and O. Zahn. Angular Power Spectra of the Millimeter-wavelength Background Light from Dusty Star-forming Galaxies with the South Pole Telescope. *ApJ*, 718:632–646, August 2010.
- [12] D. Hanson et al. Detection of B-mode Polarization in the Cosmic Microwave Background with Data from the South Pole Telescope. *Phys.Rev.Lett.*, 111(14):141301, 2013.
- [13] C. M. Hirata and U. Seljak. Reconstruction of lensing from the cosmic microwave background polarization. *Phys. Rev. D*, 68(8):083002, October 2003.
- [14] W. Hu and R. Scranton. Measuring dark energy clustering with CMB-galaxy correlations. *Phys. Rev. D*, 70(12):123002, December 2004.
- [15] M. Kamionkowski and E. D. Kovetz. The Quest for B Modes from Inflationary Gravitational Waves. *ARA&A*, 54:227–269, September 2016.
- [16] Keck Array & BICEP2 Collaborations, P. A. R. Ade, Z. Ahmed, R. W. Aikin, K. D. Alexander, D. Barkats, S. J. Benton, C. A. Bischoff, J. J. Bock, R. Bowens-Rubin, J. A. Brevik, I. Buder, E. Bullock, V. Buza, J. Connors, B. P. Crill, L. Duband, C. Dvorkin, J. P. Filippini, S. Fliescher, J. Grayson, M. Halpern, S. Harrison, G. C. Hilton, H. Hui, K. D. Irwin, K. S. Karkare, E. Karpel, J. P. Kaufman, B. G. Keating, S. Kefeli, S. A. Kernasovskiy, J. M. Kovac, C. L. Kuo, E. M. Leitch, M. Lueker, K. G. Megerian, C. B. Netterfield, H. T. Nguyen, R. O’Brien, R. W. Ogburn, IV, A. Orlando, C. Pryke, S. Richter, R. Schwarz, C. D. Sheehy, Z. K. Staniszewski, B. Steinbach, R. V. Sudiwala, G. P. Teply, K. L. Thompson, J. E. Tolan, C. Tucker, A. D. Turner, A. G. Vieregg, A. C. Weber, D. V. Wiebe, J. Willmert, C. L. Wong, W. L. K. Wu, and K. W. Yoon. BICEP2

/ Keck Array VI: Improved Constraints On Cosmology and Foregrounds When Adding 95 GHz Data From Keck Array. *Physical Review Letters*, 116(3):031302, January 2016.

- [17] R. Keisler, S. Hoover, N. Harrington, J. W. Henning, P. A. R. Ade, K. A. Aird, J. E. Austermann, J. A. Beall, A. N. Bender, B. A. Benson, L. E. Bleem, J. E. Carlstrom, C. L. Chang, H. C. Chiang, H. Cho, R. Citron, T. M. Crawford, A. T. Crites, T. de Haan, M. A. Dobbs, W. Everett, J. Gallicchio, J. Gao, E. M. George, A. Gilbert, N. W. Halverson, D. Hanson, G. C. Hilton, G. P. Holder, W. L. Holzapfel, Z. Hou, J. D. Hrubes, N. Huang, J. Hubmayr, K. D. Irwin, L. Knox, A. T. Lee, E. M. Leitch, D. Li, D. Luong-Van, D. P. Marrone, J. J. McMahon, J. Mehl, S. S. Meyer, L. Mocuano, T. Natoli, J. P. Nibarger, V. Novosad, S. Padin, C. Pryke, C. L. Reichardt, J. E. Ruhl, B. R. Saliwanchik, J. T. Sayre, K. K. Schaffer, E. Shirokoff, G. Smecher, A. A. Stark, K. T. Story, C. Tucker, K. Vanderlinde, J. D. Vieira, G. Wang, N. Whitehorn, V. Yefremenko, and O. Zahn. Measurements of Sub-degree B-mode Polarization in the Cosmic Microwave Background from 100 Square Degrees of SPTpol Data. *ApJ*, 807:151, July 2015.
- [18] M. Kesden, A. Cooray, and M. Kamionkowski. Separation of Gravitational-Wave and Cosmic-Shear Contributions to Cosmic Microwave Background Polarization. *Physical Review Letters*, 89(1):011304, July 2002.
- [19] L. Knox. Determination of inflationary observables by cosmic microwave background anisotropy experiments. *Phys. Rev. D*, 52:4307–4318, October 1995.
- [20] Lloyd Knox and Yong-Seon Song. Limit on the detectability of the energy scale of inflation. *Phys. Rev. Lett.*, 89:011303, Jun 2002.
- [21] P. Larsen, A. Challinor, B. D. Sherwin, and D. Mak. Demonstration of Cosmic Microwave Background Delensing Using the Cosmic Infrared Background. *Physical Review Letters*, 117(15):151102, October 2016.
- [22] R. Laureijs, J. Amiaux, S. Arduini, J. . Auguères, J. Brinchmann, R. Cole, M. Cropper, C. Dabin, L. Duvet, A. Ealet, and et al. Euclid Definition Study Report. *ArXiv e-prints*, October 2011.
- [23] Andrew R. Liddle and David H. Lyth. Cobe, gravitational waves, inflation and extended inflation. *Physics Letters B*, 291(4):391 – 398, 1992.
- [24] D. N. Limber. The Analysis of Counts of the Extragalactic Nebulae in Terms of a Fluctuating Density Field. *ApJ*, 117:134, January 1953.
- [25] LSST Science Collaboration, P. A. Abell, J. Allison, S. F. Anderson, J. R. Andrew, J. R. P. Angel, L. Armus, D. Arnett, S. J. Asztalos, T. S. Axelrod, and et al. LSST Science Book, Version 2.0. *ArXiv e-prints*, December 2009.
- [26] A. Manzotti, K. T. Story, W. L. K. Wu, J. E. Austermann, J. A. Beall, A. N. Bender, B. A. Benson, L. E. Bleem, J. J. Bock, J. E. Carlstrom, C. L. Chang, H. C. Chiang,

- H. Cho, R. Citron, A. Conley, T. M. Crawford, A. T. Crites, T. de Haan, M. A. Dobbs, S. Dodelson, W. Everett, J. Gallicchio, E. M. George, A. Gilbert, N. W. Halverson, N. Harrington, J. W. Henning, G. C. Hilton, G. P. Holder, W. L. Holzapfel, S. Hoover, Z. Hou, J. D. Hrubes, N. Huang, J. Hubmayr, K. D. Irwin, R. Keisler, L. Knox, A. T. Lee, E. M. Leitch, D. Li, J. J. McMahon, S. S. Meyer, L. M. Mocanu, T. Natoli, J. P. Nibarger, V. Novosad, S. Padin, C. Pryke, C. L. Reichardt, J. E. Ruhl, B. R. Saliwanchik, J. T. Sayre, K. K. Schaffer, G. Smecher, A. A. Stark, K. Vanderlinde, J. D. Vieira, M. P. Viero, G. Wang, N. Whitehorn, V. Yefremenko, and M. Zemcov. CMB Polarization B-mode Delensing with SPTpol and Herschel. *ArXiv e-prints*, January 2017.
- [27] P. Motloch, W. Hu, and A. Benoit-Lévy. CMB lens sample covariance and consistency relations. *Phys. Rev. D*, 95(4):043518, February 2017.
- [28] T. Namikawa. CMB internal delensing with general optimal estimator for higher-order correlations. *Phys. Rev. D*, 95(10):103514, May 2017.
- [29] T. Namikawa, D. Yamauchi, B. Sherwin, and R. Nagata. Delensing cosmic microwave background B modes with the Square Kilometre Array Radio Continuum Survey. *Phys. Rev. D*, 93(4):043527, February 2016.
- [30] Planck Collaboration, P. A. R. Ade, N. Aghanim, D. Alina, M. I. R. Alves, C. Armitage-Caplan, M. Arnaud, D. Arzoumanian, M. Ashdown, F. Atrio-Barandela, and et al. Planck intermediate results. XIX. An overview of the polarized thermal emission from Galactic dust. *A&A*, 576:A104, April 2015.
- [31] Planck Collaboration, P. A. R. Ade, N. Aghanim, M. Arnaud, M. Ashdown, J. Aumont, C. Baccigalupi, A. J. Banday, R. B. Barreiro, J. G. Bartlett, and et al. Planck 2015 results. XV. Gravitational lensing. *A&A*, 594:A15, September 2016.
- [32] Planck Collaboration, P. A. R. Ade, N. Aghanim, M. Arnaud, M. Ashdown, J. Aumont, C. Baccigalupi, A. J. Banday, R. B. Barreiro, J. G. Bartlett, and et al. Planck 2015 results. XV. Gravitational lensing. *A&A*, 594:A15, September 2016.
- [33] Planck Collaboration, N. Aghanim, M. Ashdown, J. Aumont, C. Baccigalupi, M. Ballardini, A. J. Banday, R. B. Barreiro, N. Bartolo, S. Basak, K. Benabed, J.-P. Bernard, M. Bersanelli, P. Bielewicz, L. Bonavera, J. R. Bond, J. Borrill, F. R. Bouchet, F. Boulanger, C. Burigana, E. Calabrese, J.-F. Cardoso, J. Carron, H. C. Chiang, L. P. L. Colombo, B. Comis, F. Couchot, A. Coulais, B. P. Crill, A. Curto, F. Cuttaia, P. de Bernardis, G. de Zotti, J. Delabrouille, E. Di Valentino, C. Dickinson, J. M. Diego, O. Doré, M. Douspis, A. Ducout, X. Dupac, S. Dusini, F. Elsner, T. A. Enßlin, H. K. Eriksen, E. Falgarone, Y. Fantaye, F. Finelli, F. Forastieri, M. Frailis, A. A. Fraisse, E. Franceschi, A. Frolov, S. Galeotta, S. Galli, K. Ganga, R. T. Génova-Santos, M. Gerbino, T. Ghosh, Y. Giraud-Héraud, J. González-Nuevo, K. M. Górski, A. Gruppuso, J. E. Gudmundsson, F. K. Hansen, G. Helou, S. Henrot-Versillé, D. Herranz, E. Hivon, Z. Huang, A. H. Jaffe, W. C. Jones, E. Keihänen, R. Keskitalo, K. Kiiveri,

- T. S. Kisner, N. Krachmalnicoff, M. Kunz, H. Kurki-Suonio, J.-M. Lamarre, M. Langer, A. Lasenby, M. Lattanzi, C. R. Lawrence, M. Le Jeune, F. Levrier, P. B. Lilje, M. Lilley, V. Lindholm, M. López-Caniego, Y.-Z. Ma, J. F. Macías-Pérez, G. Maggio, D. Maino, N. Mandolesi, A. Mangilli, M. Maris, P. G. Martin, E. Martínez-González, S. Matarrese, N. Mauri, J. D. McEwen, A. Melchiorri, A. Mennella, M. Migliaccio, M.-A. Miville-Deschênes, D. Molinari, A. Moneti, L. Montier, G. Morgante, A. Moss, P. Natoli, C. A. Oxborrow, L. Pagano, D. Paoletti, G. Patanchon, O. Perdereau, L. Perotto, V. Pettorino, F. Piacentini, S. Plaszczyński, L. Polastri, G. Polenta, J.-L. Puget, J. P. Rachen, B. Racine, M. Reinecke, M. Remazeilles, A. Renzi, G. Rocha, C. Rosset, M. Rossetti, G. Roudier, J. A. Rubiño-Martín, B. Ruiz-Granados, L. Salvati, M. Sandri, M. Savelainen, D. Scott, C. Sirignano, G. Sirri, J. D. Soler, L. D. Spencer, A.-S. Suur-Uski, J. A. Tauber, D. Tavagnacco, M. Tenti, L. Toffolatti, M. Tomasi, M. Tristram, T. Trombetti, J. Valiviita, F. Van Tent, P. Vielva, F. Villa, N. Vittorio, B. D. Wandelt, I. K. Wehus, A. Zacchei, and A. Zonca. Planck intermediate results. XLVIII. Disentangling Galactic dust emission and cosmic infrared background anisotropies. *A&A*, 596:A109, December 2016.
- [34] POLARBEAR Collaboration. A Measurement of the Cosmic Microwave Background B-mode Polarization Power Spectrum at Sub-degree Scales with POLARBEAR. *ApJ*, 794:171, October 2014.
- [35] POLARBEAR Collaboration. Evidence for Gravitational Lensing of the Cosmic Microwave Background Polarization from Cross-Correlation with the Cosmic Infrared Background. *Physical Review Letters*, 112(13):131302, April 2014.
- [36] Emmanuel Schaan, Elisabeth Krause, Tim Eifler, Olivier Doré, Hironao Miyatake, Jason Rhodes, and David N. Spergel. Looking through the same lens: Shear calibration for lsst, euclid, and wfirst with stage 4 cmb lensing. *Phys. Rev. D*, 95:123512, Jun 2017.
- [37] N. Sehgal, M. S. Madhavacheril, B. Sherwin, and A. van Engelen. Internal delensing of cosmic microwave background acoustic peaks. *Phys. Rev. D*, 95(10):103512, May 2017.
- [38] U. Seljak and C. M. Hirata. Gravitational lensing as a contaminant of the gravity wave signal in the CMB. *Phys. Rev. D*, 69(4):043005, February 2004.
- [39] U. Seljak and M. Zaldarriaga. Signature of Gravity Waves in the Polarization of the Microwave Background. *Physical Review Letters*, 78:2054–2057, March 1997.
- [40] B. D. Sherwin and M. Schmittfull. Delensing the CMB with the cosmic infrared background. *Phys. Rev. D*, 92(4):043005, August 2015.
- [41] B. D. Sherwin and M. Schmittfull. Delensing the CMB with the cosmic infrared background. *Phys. Rev. D*, 92(4):043005, August 2015.
- [42] G. Simard, D. Hanson, and G. Holder. Prospects for Delensing the Cosmic Microwave Background for Studying Inflation. *ApJ*, 807:166, July 2015.

- [43] K. M. Smith, D. Hanson, M. LoVerde, C. M. Hirata, and O. Zahn. Delensing CMB polarization with external datasets. *J. Cosmology Astropart. Phys.*, 6:14, June 2012.
- [44] D. Spergel, N. Gehrels, J. Breckinridge, M. Donahue, A. Dressler, B. S. Gaudi, T. Greene, O. Guyon, C. Hirata, J. Kalirai, N. J. Kasdin, W. Moos, S. Perlmutter, M. Postman, B. Rauscher, J. Rhodes, Y. Wang, D. Weinberg, J. Centrella, W. Traub, C. Baltay, J. Colbert, D. Bennett, A. Kiessling, B. Macintosh, J. Merten, M. Mortonson, M. Penny, E. Rozo, D. Savransky, K. Stapelfeldt, Y. Zu, C. Baker, E. Cheng, D. Content, J. Dooley, M. Foote, R. Goullioud, K. Grady, C. Jackson, J. Kruk, M. Levine, M. Melton, C. Peddie, J. Ruffa, and S. Shaklan. WFIRST-2.4: What Every Astronomer Should Know. *ArXiv e-prints*, May 2013.
- [45] A. van Engelen, B. D. Sherwin, N. Sehgal, G. E. Addison, R. Allison, N. Battaglia, F. de Bernardis, J. R. Bond, E. Calabrese, K. Coughlin, D. Crichton, R. Datta, M. J. Devlin, J. Dunkley, R. Dünner, P. Gallardo, E. Grace, M. Gralla, A. Hajian, M. Hasselfield, S. Henderson, J. C. Hill, M. Hilton, A. D. Hincks, R. Hlozek, K. M. Huffenberger, J. P. Hughes, B. Koopman, A. Kosowsky, T. Louis, M. Lungu, M. Madhavacheril, L. Maurin, J. McMahon, K. Moodley, C. Munson, S. Naess, F. Nati, L. Newburgh, M. D. Niemack, M. R. Nolta, L. A. Page, C. Pappas, B. Partridge, B. L. Schmitt, J. L. Sievers, S. Simon, D. N. Spergel, S. T. Staggs, E. R. Switzer, J. T. Ward, and E. J. Wollack. The Atacama Cosmology Telescope: Lensing of CMB Temperature and Polarization Derived from Cosmic Infrared Background Cross-correlation. *ApJ*, 808:7, July 2015.
- [46] E. L. Wright, P. R. M. Eisenhardt, A. K. Mainzer, M. E. Ressler, R. M. Cutri, T. Jarrett, J. D. Kirkpatrick, D. Padgett, R. S. McMillan, M. Skrutskie, S. A. Stanford, M. Cohen, R. G. Walker, J. C. Mather, D. Leisawitz, T. N. Gautier, III, I. McLean, D. Benford, C. J. Lonsdale, A. Blain, B. Mendez, W. R. Irace, V. Duval, F. Liu, D. Royer, I. Heinrichsen, J. Howard, M. Shannon, M. Kendall, A. L. Walsh, M. Larsen, J. G. Cardon, S. Schick, M. Schwalm, M. Abid, B. Fabinsky, L. Naes, and C.-W. Tsai. The Wide-field Infrared Survey Explorer (WISE): Mission Description and Initial On-orbit Performance. *AJ*, 140:1868–1881, December 2010.
- [47] L. Yan, E. Donoso, C.-W. Tsai, D. Stern, R. J. Assef, P. Eisenhardt, A. W. Blain, R. Cutri, T. Jarrett, S. A. Stanford, E. Wright, C. Bridge, and D. A. Riechers. Characterizing the Mid-infrared Extragalactic Sky with WISE and SDSS. *AJ*, 145:55, March 2013.
- [48] B. Yu, J. C. Hill, and B. D. Sherwin. Multi-tracer CMB delensing maps from Planck and WISE data. *ArXiv e-prints*, May 2017.
- [49] M. Zaldarriaga and U. Seljak. Gravitational lensing effect on cosmic microwave background polarization. *Phys. Rev. D*, 58(2):023003, July 1998.